Projected Hydroclimate Changes Driven by Carbon Dioxide Trends and Vegetation Modeling in CMIP6

Paul A Dirmeyer[1], Kai Huang[1], Nikki Lydeen[1], Zachary H. Manthos[1], Scott Knapp[1], and Finley Miles Hay-Chapman[1]

[1]George Mason University

November 23, 2022

Abstract

Past and projected changes in global hydroclimate in Earth system models have been examined. The Budyko framework that relates the partitioning of precipitation into evaporation to a location's aridity has been modified to account for the effect of interannual terrestrial water storage and compared to traditional methods. The new formulation better fits climate model data over most of the globe. Old and new formulations are used to quantify changes in the spatial patterns of hydroclimate based locally on year-to-year variations water and energy cycle variables. Focus is on multi-model median responses to changing climate. The changes in hydroclimate from preindustrial to recent historical (1965-2014) conditions often have different patterns and characteristics than changes due only to increasing CO_2. For simulations with gradually increasing CO_2, differing model treatments of vegetation are found specifically to have categorically different impacts on hydroclimate, particularly altering the relationship between aridity and the fraction of precipitation contributing to evaporation in models that predict vegetation changes. Models that predict vegetation phenology have consistently different responses to increasing CO_2 than models that do not. Dynamic vegetation models show more widespread but less consistent differences than other models, perhaps reflecting their less mature state. Nevertheless, there is clearly sensitivity to vegetation that illustrates the importance of including the representation of biospheric shifts in Earth system models.

Projected Hydroclimate Changes Driven by Carbon Dioxide Trends and Vegetation Modeling in CMIP6

Paul A. Dirmeyer[12], Kai Huang[2], Nikki Lydeen[2], Zachary Manthos[2], Scott Knapp[2] and Finley Miles Hay-Chapman[2]

[1]Center for Ocean-Land-Atmosphere Studies, George Mason University, Fairfax, Virginia, USA.

[2]Department of Atmospheric, Oceanic and Earth Sciences, George Mason University, Fairfax, Virginia, USA.

Corresponding author: Paul A. Dirmeyer (pdirmeye@gmu.edu)

Key Points:

- Factors other than increasing atmospheric CO2 contribute markedly to changes in hydroclimate across much of the globe
- Accounting for interannual terrestrial water storage provides a more accurate relationship between evaporation, precipitation and aridity
- Hydroclimate response to increasing CO2 significantly depends on the treatment of vegetation in Earth system models

Abstract

Past and projected changes in global hydroclimate in Earth system models have been examined. The Budyko framework that relates the partitioning of precipitation into evaporation to a location's aridity has been modified to account for the effect of interannual terrestrial water storage and compared to traditional methods. The new formulation better fits climate model data over most of the globe. Old and new formulations are used to quantify changes in the spatial patterns of hydroclimate based locally on year-to-year variations water and energy cycle variables. Focus is on multi-model median responses to changing climate. The changes in hydroclimate from preindustrial to recent historical (1965-2014) conditions often have different patterns and characteristics than changes due only to increasing CO_2. For simulations with gradually increasing CO_2, differing model treatments of vegetation are found specifically to have categorically different impacts on hydroclimate, particularly altering the relationship between aridity and the fraction of precipitation contributing to evaporation in models that predict vegetation changes. Models that predict vegetation phenology have consistently different responses to increasing CO_2 than models that do not. Dynamic vegetation models show more widespread but less consistent differences than other models, perhaps reflecting their less mature state. Nevertheless, there is clearly sensitivity to vegetation that illustrates the importance of including the representation of biospheric shifts in Earth system models.

Plain Language Summary

"Hydroclimate" means aspects of climate related to the water cycle, like the fraction of precipitation that evaporates back into the atmosphere (evaporation ratio), or how dry a location is (aridity). Such hydroclimate parameters are not independent of one another: evaporation ratio and aridity are strongly coupled via the Budyko relationship, with consequences for water resources, groundwater recharge, river flows and vegetation health. The Budyko relationship itself varies spatially due to climate, soil properties, terrain and vegetation. Hydroclimate changes in a changing climate, but vegetation adds an extra layer of complexity. We find that hydroclimate changes from only CO_2 increases do not resemble historical changes in a large suite of climate models, due to added effects from vegetation as well as aerosols and other climate forcings. As CO_2 increases, models that predict seasonal to interannual fluctuations in vegetation phenology (greenness, canopy density, etc.) have consistently different responses than simpler models that do not. Models that also predict the extinction and migration of biomes show even more widespread but less consistent differences in the evolution of hydroclimate. Careful consideration needs to be given to the role vegetation plays in hydroclimate, as water resources will not only be affected by future warming.

1 Introduction

Over periods of at least one year (i.e., neglecting the seasonal cycle), fluctuations in the storage of water below the land surface are generally small relative to the fluxes inward (precipitation) and outward (evapotranspiration and runoff). The same is true for heat, where the primary input is absorbed solar radiation, and outputs are net longwave radiation and turbulent heat fluxes. These two quasi-equilibrium budgets are linked, in that energy that escapes the land surface as turbulent latent heat flux is the energy used to remove water from the land in the form of evapotranspiration (E) into the atmosphere. The functional relationship between E, precipitation and net radiation derived by Budyko (1974) has the essential characteristics that in arid regions $R_{net}/\lambda P \gg 1$, where R_{net} is average net radiation, P is average precipitation and λ is the latent heat of evaporation. A consequence is that nearly all precipitation is lost to land as evaporation in arid regions. In humid regions where $R_{net}/\lambda P \ll 1$, E approaches its potential rate, which is limited by lack of available energy.

The quasi-equilibrium Budyko perspective is thus built around these two limits: energy limitations on E in humid regions and moisture limitations on E in arid regions (Sposito, 2017). Lacking any temporal variability in precipitation or net radiation, a location having $R_{net} = \lambda P$ might be expected to experience no limitations on E. In reality this is not the case. Locations where long-term $R_{net}/\lambda P \cong 1$ are often locations that experience a seasonal cycle that oscillates between energy and moisture limitations on E, experiencing a wet season with significant runoff and a dry season when soil moisture declines toward the wilting point. As a result, long term rates of E can be well below the limits suggested by either energy or moisture limitations (Milly, 1994). Storage of water below the land surface can moderate this seasonality, extending the hydrologic time scale and supplying more water for E and runoff during the dry season than contemporaneous precipitation would allow. Yet other physical restrictions also limit E, such as the finite depth of plant roots and plant physiological responses to environmental stresses within the diurnal cycle (Ye et al., 2015).

The assumptions and limits inherent in the Budyko relationship underpin much of the theory of land-atmosphere (L-A) interactions (Santanello et al., 2018). Namely, soil moisture can act as a regulator of surface heat fluxes, controlling the partitioning of net radiation between latent and sensible heat flux (and thus the rate of E) at places and times when net radiation is abundant. Otherwise, the available energy from net radiation is itself the controlling factor on E. Concomitant modulation of sensible heat fluxes affects boundary layer development in the lower troposphere, with consequences for atmospheric thermodynamics, convective cloud formation, and the general circulation (Betts, 2004).

Applications of the Budyko model in the phase-space portrayed by the evaporation ratio (or E ratio: E/P) as a function of aridity ($R_{net}/\lambda P$) fall into three categories. First is the local climatological application at one or more specific locations. A single location may be a flux tower where the three essential quantities P, E, and R_{net} are measured directly, a hydrologic catchment where at least P and perhaps R_{net} are measured but E is inferred from P and streamflow measurements at the exit of the catchment, or a grid cell from a climate model or ecohydrologic model. In this case, data are gathered over many years to determine a single point for the values of aridity versus E ratio space, which provides a two-parameter definition of that location's hydroclimate (Destouni et al., 2013; Oudin et al., 2008; D. Wang & Tang, 2014; L. Zhang et al., 2004).

The second category is a variation of the first, wherein *interannual* variations in E ratio versus aridity space are charted to determine the hydroclimatic variability of the location over time, typically applied at an annual time step hydroclimate (Jiang et al., 2015; R. D. Koster & Suarez, 1999; Ning et al., 2019; D. Yang et al., 2009; Hui Yang et al., 2018; Ye et al., 2015). If variations are normally distributed, means and standard deviations can provide sufficient information to characterize hydroclimatic variability in time. But frequently the time distribution of these parameters is not normal, especially for the aridity index in dry regions, which can become extremely large in drought years. Medians and quartiles provide a more robust characterization of such variability.

In the third category, the first approach is applied over many locations, and the climatological values plotted to portray the *spatial* variations of E ratio versus aridity (Carmona et al., 2016; Dirmeyer & Zeng, 1999; Greve et al., 2020; Li et al., 2018; Miralles et al., 2016; Porada et al., 2011; Xu et al., 2013). This also allows maps of aridity and E ratio to be produced (Kumar et al., 2016; Zhou et al., 2015). Furthermore, the direct relationships between other water and energy balance terms to the central Budyko variables allow for other useful applications (e.g., Koster 2015; Roderick and Farquhar 2011; Brubaker et al. 1993; Burde and Zangvil 2001).

The result of either categories 2 or 3 is a distribution of points in the $(R_{net}/\lambda P, E/P)$ plane. Many physically motivated but ultimately empirical functions have been derived to fit the distribution of points as if E/P were a monotonic function of $R_{net}/\lambda P$. Budyko's original formulation took the form:

$$\frac{E}{P} = \left[\frac{R_{net}}{\lambda P}\left(1 - e^{-R_{net}/\lambda P}\right)\tanh\left(\frac{\lambda P}{R_{net}}\right)\right]^{1/\omega_B}, \qquad \omega_B = 2.0$$

where the exponent ω_B was a fixed number. Subsequently, many formulations have been proposed in order to provide flexibility to optimize the fitting of the function to data (cf. Yang and Yang 2011). One popular formation is that of Fu as described by Zhang et al. (2004):

$$\frac{E}{P} = 1 + \frac{R_{net}}{\lambda P} - \left[1 + \left(\frac{R_{net}}{\lambda P}\right)^{\omega_F}\right]^{1/\omega_F}$$

where ω_F is a tunable parameter that implicitly represents hydrologic characteristics of the location, such as subsurface water storage capacity and seasonality in aridity. Most such tunable formulations of the Budyko relationship rely on a single parameter. Given the assumptions that the function converges asymptotically to the energy and water limits at low and high aridity respectively, the single parameter controls how closely the function conforms to the limits in the neighborhood of $R_{net}/\lambda P \sim 1$. A number of variations on the single parameter Budyko formulation have been proposed (e.g., Choudhury 1999; Zhang et al. 2001, 2004; Wang and Tang 2014) with the goal of better fitting the relationship to observed data for various applications.

As the tuning parameter effectively moves the fitted curve closer or farther from the limits described above, the parameter itself becomes an index of the hydroclimatology described by annual mean fields of precipitation, ET and net radiation at a given location. In a changing climate, wherein assumptions of hydrologic stationarity are violated (Milly et al., 2008, 2015), there is no reason to assume that the hydroclimatological distributions described by the Budyko relationship should not change as well. Previous studies have examined this using climate model simulations from the fifth Climate Model Intercomparison Project (CMIP5; Taylor et al. 2012) to quantify future hydrologic sensitivity (Kumar et al., 2016; Singh & Kumar, 2015), spatial hydroclimate variability (category 3 above; Li et al. 2018), and projected runoff changes (Milly & Dunne, 2016; Osborne & Lambert, 2018; Zheng et al., 2018). However, application of the parameter itself as an index of hydroclimatic change has been limited. Yang et al. (2018) recognized the application of such an index as an indicator of the water retention characteristics at the catchment scale, as well as noting the potential influence of vegetation responses to increasing CO_2 and temperature as a factor in its change. In fact, many different possible influences are agglomerated into such a single parameter.

In this study, we examine the use of such a hydroclimatic index taken as a single parameter from various formulations of the Budyko relationship as an integrative indicator of climate change impacts on the hydrologic cycle. Using data from CMIP6 (Eyring et al., 2016), we examine how the hydroclimatological position and interannual variability in Budyko space of any location may change from past to present and as a result of ever-increasing greenhouse gas concentrations in the atmosphere. We examine how well different climate models agree on the positions and spatial patterns of the hydroclimatic index estimated from a best fit to model data, using a curve-fitting procedure at each location through yearly values in Budyko space, and determine multi-model consensus estimates. Finally, we attempt to attribute changes in aridity, E ratio and the ω parameter to changes in CO_2 and vegetation.

The data used, models considered, and analysis methods are described in section 2. Results are shown in sections 3 and 4, showing first the variability of aridity and E ratio, then examining three formulations of the Budyko curve to synthesize hydroclimate impacts. The potential role of vegetation and its simulation in different Earth system models is examined in section 5, and a summary of results is presented in section 6.

2 Methodology and Data

2.1 Fitting of Budyko formulations

Using annual mean data calculated from the monthly output of 37 CMIP6 models (see Tables 1 and S1), we find median values and interquartile ranges (IQR) of both aridity and E ratio for every land grid cell on each models' native output grid for each of four periods taken from three DECK simulations described below. We also use the time series of annual values of aridity and E ratio to produce scatter plots in Budyko space through which several different single parameter formulations of the Budyko relationship are fit, using a basic least-squares difference minimization approach to find the optimum value of the ω parameter.

Several different formulations are explored. The Fu formulation described above has been used in this curve-fitting context in many previous studies and we use it here, estimating values of the parameter ω_F as a function of location for each model and experiment situation described below. We also use the original Budyko formulation but allow the parameter ω_B to vary so that it can be used for better fitting of the function.

Because of the extreme heteroscedasticity of data in Budyko space at many locations, obtaining a good fit to the data is challenging. That was a primary motivation for exploring more than one formulation. Furthermore, we have found that specific formulations tend to perform better in some climate regimes than others. Here we describe problems faced in applying the Fu and modified Budyko formulations, and how that has led us to a novel formulation that appears to fit the range of data best. All three are used in our analyses and are ultimately compared.

As mentioned above, the classical Budyko relationship depicts evaporation ratio E/P as a function of aridity $R_{net}/(\lambda P)$. In this framework. Hydroclimatological limits suggest that for any period with a duration of an integer number of years ≥1, $E/P \leq R_{net}/(\lambda P)$ for $R_{net}/(\lambda P) < 1$, and $E/P \leq 1$ for $R\_net/(\lambda P) > 1$. For CMIP6 models, the first limit appears to be obeyed rather firmly but the second frequently is not. So, in all cases, points that exceed $E/P > 1.2$ are removed from the sample before parameter optimization. Also, over very dry locations, extremely large values of $R_{net}/(\lambda P)$ can result – often exceeding 100. Points at such high aridity can greatly impact the curve fitting, so all values of $R\_net/\lambda P > 8$ are also removed from the sample. For purposes of representing the Budyko framework, it is the values of E ratio closer to $R_{net}/\lambda P \sim 1$, where the second derivative of fitting functions is largest, that provide the most information about the effects of soil water retention, vegetation, etc., on E – runoff partitioning (Kumar et al., 2016).

Some examples of fits through data at single points are shown in Figure 1. We find that the Fu formulation does very well in wet and moderate regions but struggles in arid locations. It appears that often the E ratio begins dropping at relatively high values of aridity, nor does it appear to asymptotically approach the $E/P = R_{net}/(\lambda P)$ limit in wetter situations. This may be due to a propensity for rainfall in such arid regions to come in infrequent but heavy downpours that contribute to large runoff, or easily permeate sandy soils becoming unavailable to evaporation. However, the Budyko formulation with a variable exponent ω_B attains something of a sigmoid shape for $\omega_B < 2$, which nicely adapts to the data distributions in arid locations.

Conversely, the variable exponent Budyko formulation struggles to fit data from humid regions, especially when there are frequently values of $E/P > 1$. The best fit is often attained for values of $\omega_B > 2$, wherein the fitted curve violates the energy-constrained limit $E/P \leq R_{net}/(\lambda P)$. These problems prompted a search for a new formulation that would work well in all climates.

We found that applying a moving average of 3 or 5 years lessened but did not remove instances of $E/P > 1$ for most models in most locations, yet removed variability, suppressed the tails in the distribution along the aridity axis, and reduced the number of degrees of freedom in the time series hampering statistical significance. Annual $E/P > 1$ is an indicator of substantial water storage, which is a hydrological characteristic of the system that should not be completely removed from consideration. Since years having $E/P > 1$ appear to be a common occurrence, we relaxed the constraint that the function must not exceed unity, although an asymptotic approach to unity is a clearly desirable characteristic for semiarid and arid climates. The best formulation we found was another slight variant on the original Budyko formula:

$$\frac{E}{P} = \frac{R_{net}}{\lambda P}\left(1 - e^{-R_{net}/\lambda P}\right)\tanh\left(\frac{\lambda P}{R_{net}}\right)\omega_Z$$

Here, the parameter ω_Z is a multiplicative factor rather than in an exponent. It retains the sigmoid at small aridity values, approaches the limit $E/P = 1$ for $\omega_Z \leq 1$, but is free to exceed that limit for $\omega_Z > 1$. Example results for this Budyko formulation without the E/P constraint are shown in the bottom row of Figure 1.

2.2 CMIP6 model data

We use output from three of the DECK experiments: piControl, historical, and 1pctCO2. However, there are four distinct periods and situations for which indices are calculated:

1. All years from piControl (~600 years): PI
2. The last 50 years of historical, representing late 20th and very early 21st century conditions): H_{L50}
3. Years 21-70 of 1pctCO2, which will lie in the range of 21st century CO2 levels, out to circa 2070 based on current projections: $1\%_{21\text{-}70}$
4. Years 91-140 of 1pctCO2, which approach the 4xCO2 levels, representing the first half of the 22nd century if little is done to ameliorate emissions: $1\%_{91\text{-}140}$

The historical simulation differs from the others in that it includes not only greenhouse gas forcings, but also observed land use changes, detailed trends in volcanic and anthropogenic aerosols, trace atmospheric constituents and solar forcing. With these four temporal samples, differences found between specific pairs are indicative of specific changes and sensitivities in the hydroclimate at locations for the various models. Specifically, we consider several pairings that address the following questions:

1. How has the hydroclimate changed since pre-industrial times [H_{L50} – PI]?
2. How is hydroclimate affected by a steady increase in atmospheric CO_2 to an approximate doubling [$1\%_{21\text{-}70}$ – PI]?
3. How might hydroclimate change from a doubling to a quadrupling of atmospheric CO_2 [$1\%_{91\text{-}140}$ – $1\%_{21\text{-}70}$]?

To keep all models on equal footing, only one ensemble member from each model is included (r1i1p1f1, unless that member is not available, in which case the next lowest variant that is available for all variables in an experiment is used – see Table 1 for details). Past results with CMIP5 suggest such indices are rather robust within experiments and not sensitive to the choice of ensemble member, nor the use of all members, when compared to differences between experiments or between models. Furthermore, the majority of the experiments for the models only provide a single simulation, so this choice puts all models on an equal footing regarding sample size.

Most models predict intraseasonal, seasonal and interannual variations in vegetation coverage and greenness, referred to as vegetation phenology. Several include a dynamic vegetation model (DVM) that can simulate the multi-year evolution and migration of biomes in response to climate changes (see supplemental Table S1). Not all the models' treatments of vegetation could be determined, as discussed in section 5.

At the time of analysis, 37 models provided the monthly mean data required to depict the three necessary quantities for describing model hydroclimatology in Budyko space, namely total precipitation (CMIP variable: pr), total evaporation (expressed as a latent heat flux: hfls) and net radiation (estimated as the sum of hfls and sensible heat flux: hfss). Note that in several instances, more than one version of a model from the same institution is included. It can be debated whether, in multi-model analyses, each model should be given equal weight or rather each institution, as there is often great similarity between results from related models. We note that the models used by many institutions are themselves descended from a small number of pioneering Earth system modeling efforts. Thus, the genetic differences, so to speak, among models are not simply discerned by the institution names listed here. We present multi-panel depictions of results from all models in the supplemental material for visual comparison, so the reader can judge the degrees of diversity represented among model results.

2.3 Multi-model analysis

In order to perform direct comparisons and produce multi-model statistics, median and IQR of aridity, E ratio, and estimates of ω_B, ω_F and ω_Z are interpolated to a common high-resolution longitude by Gaussian latitude grid (2560 x 1280 grid cells) to preserve the spatial detail and coastlines of each model (Dirmeyer et al., 2013b). A nearest-neighbor interpolation is used for each model including only land grid cells from each model; at least 90% of the models must project an ice-free land cell into each high-resolution grid cell for the value to be retained – otherwise it is assumed to be an open water or ice covered point and is masked.

Multi-model statistics are mainly based on medians to prevent outlier models from overly affecting the multi-model result. When examining the changes in the five file pairings described above, three approaches have been examined at each grid cell. The simple change in the multi-model median has been considered but found to be rather noisy. The median of the 37 changes in the individual models is found to give a more robust depiction of changes. Finally, the method of Dirmeyer et al. (2013a,b) has been used to determine the number of models showing a change of a particular sign, regardless of magnitude, and the significance of the distribution. The null hypothesis for the final method is that the change projected by each model is a random fair coin toss. Each possible split $n : 37 - n$ has an associated probability of occurring by chance, which provides a significance of consensus that complements the changes in medians used to quantify the magnitudes of changes.

3 Aridity and Evaporation Ratio

Before investigating the Budyko curve estimations, we first examine the climatologies of aridity and E ratio. Figure 2 shows, for the PI experiment, the multi-model median of these two quantities, along with the inter-model standard deviation and the normalized difference between the mean and median. The last quantity is an indication of skewness in the distribution across models. Given that the Budyko relationship describes a monotonic relationship between aridity and E ratio, it is no surprise that the maps of their medians are very similar. Humid regions have low values of both aridity and E ratio and dry regions have high values. Semi-humid to semi-arid transition regions tend to have high values of E ratio but relatively moderate aridity, reflecting the classical shape of the Budyko curve. Figures S1 and S2 show the temporal medians for each model – the multi-model statistics are calculated from the individual model medians.

The pattern of standard deviation of these quantities among models in Figure 2 largely mirrors their magnitudes. The difference between multi-model mean and median, normalized by standard deviation, shows some interesting patterns. For aridity this quantity is predominantly positive, indicating a positive skewness, i.e., there are a few models that tend towards very large values of aridity. This is especially strong over the desert regions of North Africa and Asia, but also over much of India, regions in and around the Andes, and relatively semi-arid regions surrounding the Ethiopian highlands. For E ratio, weak negative values cover most land areas, suggesting a negative skewness in the distribution across models. The notable exception is across the core of the Sahara where strong positive skewness extends. There are also areas of strong positive values along coastal margins of deserts, which could reflect large variations among models' quantification of dew and its evaporation where oceanic winds carry humid air over arid coastlines. However, these may also be an artifact of model treatments of coastal points or inaccuracies in our determination of land-sea masks for some models that did not supply such information, we cannot rule out that oceanic evaporation for some models may be counted as terrestrial. The investigation of skewness of the distributions provides another reason to focus on medians throughout this study.

Figure 3 depicts the year-to-year variability in PI for the aridity and E ratio at each location, again shown in terms of multi-model median, inter-model standard deviation and the normalized difference between the mean and median. The quantity used is inter-quartile range (IQR) – the difference between the 75th and 25th percentile in the distribution of all annual values across all years of the piControl simulation for each model. The spatial pattern of the multi-model median of IQR for aridity closely resembles the median and standard deviation from Figure 2, but the IQR for E ratio is rather different. Whereas aridity IQR appears large across all arid regions, for E ratio it is largest around upper Egypt and lands surrounding the Persian Gulf and Arabian Sea. Most arid regions have relatively modest IQR for E ratio, on par with semi-arid and humid regions.

Inter-model standard deviation for IQR is again highest in arid regions, but more limited in extent for E ratio. India is again an area of pronounced disagreement among models, given that much of it is not arid. Model agreement is high for both quantities in tropical rainforest areas, west-central China, the Canadian Rockies, Quebec and Scandinavia. Skewness tends to be large and positive over many areas for aridity IQR over arid and semi-arid regions, but also mountainous and coastal regions of South America, yet generally low over North America and Europe. For the IQR of E ratio, skewness in the model distribution is large and positive over the Sahara, southeastern Arabia, the coasts of southwestern Asia including the Indus valley, and the Tarim Basin.

Changes from past to present and for different intervals along the 1pctCO2 experiment for aridity and E ratio are shown in Figures 4 and 5 respectively. Changes are displayed in two ways – as the median of changes among all models, and as the fraction of models displaying a positive or negative change, colored by the likelihood of such a distribution occurring by chance. The latter gives a clear indication of significance of agreement among models, while the former conveys information about the magnitude of the change.

Aridity changes are large but often rather meaningless over the interior of North Africa and Arabia, given the very large medians and standard deviations there already; strong coloring in the bottom panels suggest where changes may be consequential. For instance, ongoing increases in aridity along the coastal regions of North Africa and the Mediterranean appear to be significant.

For H_{L50} – PI there are generally decreases in aridity and accompanying E ratio over large areas of the Northern Hemisphere that include forest regions in North America and Eurasia, and areas that experienced expanded agriculture: much of the Indian subcontinent, eastern China, central North America, and much of central and eastern Europe extending east across the Eurasian steppes. The decrease in aridity is especially strong in magnitude over the upper Indus Basin, but that region, like much of the Indian subcontinent, mainly sees an increase in E ratio, possibly due to the increased irrigation being correctly represented in many of the climate models. At lower latitudes, there is strong consensus for a decrease in aridity over much of tropical Africa, the Pampas of South America and Uruguay, as well as parts of western Australia. E ratio also decreases over the Nordeste region of Brazil, but increases over the eastern Amazon Basin, the Orinoco Basin, and across much of the subtropics.

The trends in the two intervals of the 1pctCO2 case, $1\%_{21\text{-}70}$ – PI (middle columns of Figures 4 and 5) and $1\%_{91\text{-}140}$ – $1\%_{21\text{-}70}$ (right columns of Figures 4 and 5), resemble each other with the main difference being changes in the later interval are generally stronger. Some of these features are seen in H_{L50} – PI as well, but some are not. For instance, the broad areas of decreasing aridity and E ratio over much of North America, Eurasia and central Australia in H_{L50} – PI reverse to increases in $1\%_{21\text{-}70}$ – PI. All three show decreasing aridity over the Indus Valley, although there is great variability in model agreement patterns over South Asia among intervals. All show decreasing aridity and E ratio over central Africa. Aridity also decreases over much of China, Patagonia and the Pampas, while E ratio decreases over the Nordeste. All show increasing aridity and E ratio over Mesoamerica, northern South America, the Mediterranean and much of southern Africa.

For the two intervals that represent pathways of a changing climate from preindustrial conditions, we see some similarities that may be attributable to comparable increases in atmospheric CO_2. The CO_2 concentration in $1\%_{21\text{-}70}$ is greater than in H_{L50}, averaging 447.2 ppm in the 50-year period versus 354.2 ppm in H_{L50}, and indeed the common features are generally stronger for $1\%_{21\text{-}70}$ – PI than for H_{L50} – PI. The different features noted may be due to the additional forcings in the historical experiment – this is explored further in section 5.

4 Budyko Curves

Next, the spatial distributions of the shape of the three Budyko curves, specified by different one-parameter formulations, are investigated. There is not a one-to-one correspondence between the magnitude of the parameters ω_B, ω_F and ω_Z, so we emphasize the spatial patterns over their values. However, each has the same general characteristics such that for lower parameter values, the curve sits lower in Budyko-space, i.e., a lower value of E ratio for a given value of aridity. For high parameter values, the curve approaches $E/P = R_{net}/\lambda P$ when $R_{net}/\lambda P < 1$. For the variable exponent Budyko formulation and Fu formulation, large parameter values lead to $E/P \to 1$ when $R_{net}/\lambda P > 1$, but this limitation is not in place for the formulation without the upper limit on E/P (see Figure 1).

Figure 6 shows the multi-model median values of, from left to right, ω_B, ω_F and ω_Z, as well as the standard deviation among models of the median, and the skewness index described previously. All three formulations tend towards low values of ω over arid regions, and high values in tropical forests. Beyond that there are some stark differences. Outside the tropics, the Budyko formulation with the tunable exponent has the highest values of ω_B in transitional regions, not the most humid locations. The Fu formulation places the lowest values of ω_F in mountainous and Arctic locations, not in deserts. Some of the lowest values of ω_F are in extratropical rainforests. The Budyko formulation without the E/P constraint tends to resemble a map of R/P in spatial pattern, where R is runoff. Interestingly, it also results in much smoother spatial patterns compared to the other formulations, and except for alpine and arctic climates it has much reduced inter-model variability (middle row of Figure 6). Estimates of ω_B and ω_F show global positive skewness (bottom row of Figure 6) whereas ω_Z shows a mix of positive and negative skewness, with pronounced negative skew over the Sahara and Arabia.

Figure 7 shows which of the three formulations has the best fit at each location, quantified as the lowest root mean square error (RMSE) of the curve through all yearly points in the Budyko space (E/P versus $R_{net}/\lambda P$). The RMSE maps for each formulation are shown in Figure S3. The Budyko formulation without the E/P constraint is the best formulation in the majority of locations, especially in the subtropics and areas that are not at either extreme (not very wet nor arid). The Budyko formulation with tunable exponent is generally most trustworthy in arid regions and a number of high-latitude locations. The Fu formulation is particularly good across northern Europe, some tropical regions, and a smattering of other locations. It should be noted that the Budyko formulation without the E/P constraint will necessarily have $\omega_Z \lesssim 1$ in locations where aridity $R_{net}/\lambda P > 1$ predominates and will have $\omega_Z > 1$ where $R_{net}/\lambda P < 1$ even when $E/P < 1$ is always true. This is because the fitting of the function to the distribution of points is optimized in these situations.

Figure S4 gives a pairwise comparison of the multi-model median values of RMSE of the best fit for the three formulations in the Budyko-space (E/P versus $R_{net}/\lambda P$) as a set of three scatter diagrams for all land grid cells in the PI case. The coloring shows the median aridity of each grid cell; RMSE generally increases with aridity, as was also evident in Figure S3. The left panel compares the Fu formulation to the variable exponent Budyko formulation. There is little overall advantage of one formulation over the other, but the preponderance of dark blue points toward the upper left-hand corner illustrates how the Fu formulation struggles in some wet climates. It also tends to do slightly more poorly in fitting very dry climates (pink) but tends to be better in the semi-humid to semi-arid regime (green). The other two panels of Figure S4 compare the new unconstrained Budyko formulation (y-axis) to the others. While the fit is generally a bit poorer in very humid regions, it tends to excel in all others except some very arid locations relative to the original Budyko formulation with the tunable exponent.

As a final measure of the goodness of fit of each of the formulations, Figure S5 shows the displacement of the multi-model median values of aridity and E ratio from the nearest point on the best fit Budyko curve using the multi-model median value of ω. Because of the nonlinear nature of the Budyko curves, there is no expectation that the means should fall on the curve, let alone the medians. Nevertheless, we see for all three formulations the displacement in Budyko space tends to be large in arid regions, moderate in semi-arid regions, and highly variable elsewhere.

Changes in the ω parameter between CMIP6 experiments for each formulation of the Budyko curve are shown in Figure 8. There are common features to each formulation: A broad reversal in changes between the Northern Hemisphere versus low latitudes and the Southern Hemisphere, and many regional features. As with aridity and E ratio, the global pattern of changes in $1\%_{91\text{-}140}$ – $1\%_{21\text{-}70}$ are largely an amplified version of the changes in $1\%_{21\text{-}70}$ – PI, yet the resemblance between $1\%_{21\text{-}70}$ – PI and H_{L50} – PI is limited.

There is a tendency for relatively stronger changes at higher latitudes than low latitudes in ω_Z for H_{L50} – PI, whereas the other two formulations have more evenly distributed magnitudes of changes around the globe. Specifically, ω changes have similar patterns between the tunable Budyko formulation and the Fu formulation, but the Budyko formulation without the E/P constraint differs in many areas. Recalling that an increase in ω connotes a relationship between E/P and $R_{net}/\lambda P$ hews closer to the energy limits for all three formulations, the relationship moves closer to the water limit incidentally for ω_Z only where $\omega_Z \lesssim 1$. For $\omega_Z > 1$ the moisture constraint is neglected. Thus, we see an increase in ω_Z over much of the eastern US for H_{L50} – PI but decreases in ω_B and ω_F. If we look instead at the significance in the agreement among models (Figure 9), the discrepancies do not look as stark. Where signs of changes for ω_Z disagree with the other formulations, typically one or the other formulation is not significant. The three formulations agree most for the $1\%_{91\text{-}140}$ – $1\%_{21\text{-}70}$ changes, which also have the strongest and most widespread significant shifts in ω. For H_{L50} – PI and $1\%_{21\text{-}70}$ – PI there is strong resemblance between patterns for ω_B and ω_F, while ω_Z has clear differences concentrated in more humid regions of the globe.

5 Interpretation of the Role of Vegetation

As noted earlier, the historical experiment contains many more specified climate drivers than the DECK experiments. As a result, we see changes from PI to H_{L50} differ from those in PI to $1\%_{21\text{-}70}$ in many locations (Figures 4, 5, 8 and 9). Clearly the other forcings are exerting more impact on hydroclimate than are greenhouse gas changes. Disentangling the specific drivers of hydroclimatic shifts in CMIP6 simulations is beyond the scope of this study. There are model intercomparison projects that investigate such impacts in more detail; those relevant to hydroclimate namely involve land use change (LUMIP; Lawrence et al. 2016) and soil moisture variations (LS3MIP; van den Hurk et al. 2016).

However, there is sufficient information to sort most models based on how they simulate vegetation. Some portion of the changes seen in the historical experiment come from progressive land use change. In the DECK experiments, the only specified evolving boundary condition is atmospheric CO_2 concentration, but other components of the Earth system can evolve in response including, if a model's land surface scheme allows it, vegetation.

The CMIP6 models fall into three distinct categories regarding vegetation modeling: those that include predicted phenology and dynamic vegetation (9 models); those that include only predicted phenology (13 models), and those that have neither (8 models). Specific model information is included in Table S1 in the supplementary material, including a fourth category excluded from this part of the analysis: models for which this information could not be reliably determined from discovered published literature (7 models).

We group model results into the first three categories to isolate the hydroclimate responses to predicted phenology and dynamic vegetation. Studies have suggested vegetation variations can be an important determinant for changes in the Budyko parameter ω (Donohue et al., 2012; Ning et al., 2019; S. Zhang et al., 2016, 2018). Changes in hydroclimate can be expressed in Budyko space in terms of variations or trends in aridity and E ratio relative to the Budyko curve (Jiang et al., 2015; D. Wang & Hejazi, 2011). Specifically, changes can be visualized as having two perpendicular axes – one parallel to the Budyko curve, and one perpendicular to it (D. Yang et al., 2009). Variations along the first axis imply that the curve itself is unchanging over time (i.e., the estimated value of ω is fairly constant) and any trends in the distribution of aridity and E ratio amount to a translation along the curve. Changes perpendicular to the Budyko curve imply the value of ω is changing. Figure 10 illustrates such changes schematically, keeping in mind that there is not perfect consistency between changes in multi-model median ω (shifts in Budyko curves) and changes in multi-model median aridity and E ratio (Figure S5).

Yang et al. (2009) have suggested that movement along the Budyko curve represents changes in the climate but not in the landscape, whereas a shift normal to the Budyko curve indicates the natures of water storage, evapotranspiration and/or runoff have changed. For example, a shift in vegetation, changes in soil properties, active management of water resources or land use changes including agricultural expansion ought to alter the value of ω more than changes in mean temperature, humidity, precipitation or soil moisture. Thus, the role of vegetation in climate change ought to project predominantly on the perpendicular component.

To understand hydroclimatic changes in this context, we have taken the multi-model median values of aridity and E ratio at each grid cell for each CMIP6 experiment and the estimated values of ω_B, ω_F and ω_Z from their corresponding formulations, and decomposed the three temporal changes (H_{L50} – PI, $1\%_{21\text{-}70}$ – PI, and $1\%_{91\text{-}140}$ – $1\%_{21\text{-}70}$) into changes parallel and perpendicular to the Budyko curve. The following process is used, also portrayed in Figure 10. First, because the median values of aridity and E ratio are not guaranteed to be a point that lies exactly on the best fit Budyko curve (Figure S5), the nearest point on the Budyko curve is found, and the slope of the Budyko curve at that point is used to establish a rotation of axes. For most points along the curves for all three formations, changes parallel to the curve correspond mainly to changes in aridity, increasingly so as aridity increases. However, for low aridity the slopes of the curves become steeper and the E ratio projects more strongly onto the axis parallel to the curve. For the Budyko formulation without the E/P constraint, as well as the variable exponent Budyko formulation when $\omega_B < 2$, the curves flatten out again at very low aridity (see Figure 1).

The rotated axes are translated so the origin is at the point of median aridity and E ratio for the earlier time period of each climate change comparison. The change in Budyko space to the new median for the later period is then reckoned as a distance parallel to the Budyko curve and a distance perpendicular to the curve. Figure S6 shows the ratio, parallel distance over perpendicular distance, for each formulation and the three change intervals. In each row, grid cells are only shown where the direct distance between the two median points is less than 2 times the standard error estimated from the multi-model median year-to-year variability during the earlier of the two periods. Masked out areas are considered not to be distinguishable from natural variability. Most changes are, in Budyko space, parallel to the estimated Budyko curve for the location. There is very little perceptible difference between maps for the different formulations. Overall, while shifts along the Budyko curve predominate, their relative magnitude tends to follow aridity itself, consistent with Figures 4 and 5. It is also apparent from the separate components (Figures S7 and S8) that movement along the Budyko curve, due to its overall positive slope, corresponds to synchronized increases or decreases in both aridity and E ratio.

Figure 11 shows how changes in ω_Z between the indicated pairs of experiments differ among models without predicted vegetation phenology or dynamic vegetation (left column), with predicted phenology but no dynamic vegetation (middle column) and with both dynamic vegetation and predicted phenology (right column). We use the significance in agreement among models projecting changes in ω_Z of the same sign to try to ameliorate the smaller sample sizes and the plethora of other differences between models.

There are significant regional changes of either sign as a result of both predicted phenology and DVMs, and there is more similarity in patterns within columns (i.e., in the evolution from PI to $1\%_{21\text{-}70}$ to $1\%_{91\text{-}140}$) than across columns. There appears to be a significant decrease in ω_Z over western Europe, coastal Australia, Mesoamerica, northern South America and much of southern Africa. Systematic increases are mainly confined to eastern Asia at middle and high latitudes. Broadly, models without any prognostic vegetation component (left column) show the weakest changes in ω_Z in most locations. Regions where changes are consistent in sign and significance across both time intervals are more likely to be genuine, but the global field significance (area of change of a particular sign and significance compared to what would be expected by random chance) is marginal, especially for decreases in ω_Z. Increases over many cold-winter regions are likely the signature of changes in annual snow cover affecting water storage – a process largely independent of vegetation.

The inclusion of predicted phenology in climate models appears to have a profound effect in the Amazon Basin, where models strongly agree on a decrease in ω_Z over a large area. Otherwise, there are many scattered locations of changes of both signs that cover much more area than in the left column. Addition of a DVM (right column) leads to additional significant (90% confidence or better) changes over about two-thirds of ice-free land, but no large areas of extremely high significance as seen in the middle column. This may reflect the less mature status of dynamic vegetation modeling compared to phenology modeling, and thus reduced consistency among the climate models including DVMs. Lastly, the tendency for changes in the $1\%_{91\text{-}140}$ – $1\%_{21\text{-}70}$ case to be stronger than for $1\%_{21\text{-}70}$ – PI is weak in this analysis.

If changes in climate alone result in changes of aridity and E ratio that tend not alter ω, while landscape changes shift values of ω, there should be evidence by recalculating changes in Budyko space relative to axes parallel and perpendicular to the Budyko curve sorted by the sophistication of model vegetation parameterizations. Figures 12 and 13 show the ratio of changes (parallel over perpendicular) respectively comparing models with and without predicted phenology, and having predicted phenology but with and without DVMs. The right column of each figure shows the ratio of the ratios. Blue colors (ratios less than 1) indicate that shifts perpendicular to the Budyko curve, which result in changes in ω_Z, are larger than shifts along the curve. In the left two columns, which show the changes for the indicated subsets of models, the majority of significant changes are colored in shades of red, suggesting that overall, the shifts in hydroclimate are predominantly attributable to changing climate. However, we would expect more blue area in models with predicted phenology than without (Figure 12), and that is in fact evident in both time intervals. The histograms of the area in each ratio range help display this. Furthermore, the ratio of ratios (right column) tends to be predominantly blue: there is significantly more area < 1 than > 1. Similar results are seen for the effect of DVMs (Figure 13) although interestingly the tendency for hydroclimatological shifts perpendicular to the Budyko curve is not as strong as for the impact of predicted phenology. Nevertheless, the skewness in the histograms in the right column is also significant, suggesting DVMs also increase the likelihood of changes in ω_Z.

6 Conclusions

37 CMIP6 models have been examined regarding their portrayal of changes in hydroclimate, quantified via the Budyko framework that relates the partitioning of precipitation into evaporation at any location to that location's aridity. Alongside traditional formulations of

the Budyko equation, we have employed a new formulation that accounts for the fact that frequently evaporation is not constrained by total precipitation on annual time scales due to various terrestrial reservoirs of moisture (Figure 1). We have quantified the multi-model climatology (Figures 2, 3, 6) and changes in aridity $R_{net}/(\lambda P)$, evaporation ratio (E/P) and the parameter quantifying the local climatological relationship (ω) between the two across the models for preindustrial, historical, and projected 1% per year increases in atmospheric CO_2 concentration, concentrating on multi-model medians and degree of model consensus (Figures 4, 5, 8, 9). The Budyko formulation without the E/P constraint provides the best fit to data over more than half of the globe compared to two other common formulations (Figure 7).

We find that changes from preindustrial to recent historical (1965-2014) conditions are often inconsistent with changes ascribable only to increasing CO_2. The historical simulations include many other factors including atmospheric aerosols and land cover changes. We are able to use model documentation to determine for most models whether or not they predict vegetation phenology (rather than prescribe it as a boundary condition) and whether they employ dynamic vegetation models (DVMs) that predict spatial changes in biomes in response to changing climate. Theory suggests different meanings for changes in aridity and E ratio along the Budyko curve than perpendicular to it, with perpendicular trends being ascribed to changes in landscape (Figure 10).

There are clear differences in hydroclimate response depending on model treatment of vegetation (Figure 11). CMIP6 models with predicted vegetation phenology consistently show significantly larger changes in hydroclimate perpendicular to the Budyko curve, with a high degree of inter-model consensus over large parts of the globe (Figure 12). The implication is that models that do not predict phenology may be missing a key aspect of climate change. Models containing DVMs also show widespread differences from those that do not, but the degree of consensus among models is weaker (Figure 13). This may reflect the less mature state of these models, which have not yet converged toward consistent and accurate representation of biome responses to disturbance and climate change. Nevertheless, there is clear sensitivity that points to the importance of representing biospheric shifts in Earth system models.

There are several caveats regarding the potential role of vegetation in this comparison. First, the treatment of vegetation is far from the only difference among these sets of models. However, it is unlikely that other parameterization differences would sort out exactly along the same lines as vegetation, so vegetation should contribute most of the signal determined. Second, the number of models in each category is different, so while variations in significance thresholds are accounted for, signal and noise in each set varies as well. Third, phenology and especially dynamic vegetation are not represented in the same way across models, so responses to climate change may not be consistent. This may account for more widespread but less consistent impact of the inclusion of DVMs on projected hydroclimate. Furthermore, we refrain here from validating any model or group of models as more accurate. There is a growing body of literature on ecological emergent constraints that provide convincing evidence for such vegetation-climate connections (Cox et al., 2013; Fisher et al., 2018; He et al., 2020; Lian et al., 2018; X. Wang et al., 2020; Wu et al., 2015). Nevertheless, we conclude that vegetation modeling is an important but possibly underappreciated aspect of climate change projections that can have important consequences for adaptation, especially regarding water resources and land management.

Acknowledgments, Samples, and Data

We thank the climate modeling groups cited in Tables 1 and S1 for making their model output available, the Earth System Grid Federation (ESGF) for archiving the data and providing access, and the funding agencies who have supported CMIP6 and ESGF. Data are available via the digital object identifiers listed in Table 1. We also acknowledge the World Climate Research Programme (WCRP) Working Group on Coupled Modelling (WGCM), which is responsible for CMIP6 coordination and promotion.

Data processing and preliminary analyses for this study were performed by the co-authors as part of a graduate class project in land-climate interactions in the Climate Dynamics Program of George Mason University, Fairfax, Virginia, USA. The lead author's synthesis of the student material was supported by funding from the National Science Foundation (AGS-1338427) for the Center for Ocean Land Atmosphere Studies (COLA).

References

Betts, A. K. (2004). Understanding Hydrometeorology Using Global Models. *Bulletin of the American Meteorological Society*, *85*(11), 1673–1688. https://doi.org/10.1175/BAMS-85-11-1673

Brubaker, K. L., Entekhabi, D., & Eagleson, P. S. (1993). Estimation of Continental Precipitation Recycling. *Journal of Climate*, *6*(6), 1077–1089. https://doi.org/10.1175/1520-0442(1993)006<1077:EOCPR>2.0.CO;2

Budyko, M. I. (1974). *Climate and Life*. New York, NY, USA: Academic Press.

Burde, G. I., & Zangvil, A. (2001). The Estimation of Regional Precipitation Recycling. Part II: A New Recycling Model. *Journal of Climate*, *14*(12), 2509–2527. https://doi.org/10.1175/1520-0442(2001)014<2509:TEORPR>2.0.CO;2

Carmona, A. M., Poveda, G., Sivapalan, M., Vallejo-Bernal, S. M., & Bustamante, E. (2016). A scaling approach to Budyko's framework and the complementary relationship of evapotranspiration in humid environments: case study of the Amazon River basin.

Hydrology and Earth System Sciences, *20*(2), 589–603. https://doi.org/10.5194/hess-20-589-2016

Choudhury, BhaskarJ. (1999). Evaluation of an empirical equation for annual evaporation using field observations and results from a biophysical model. *Journal of Hydrology*, *216*(1), 99–110. https://doi.org/10.1016/S0022-1694(98)00293-5

Cox, P. M., Pearson, D., Booth, B. B., Friedlingstein, P., Huntingford, C., Jones, C. D., & Luke, C. M. (2013). Sensitivity of tropical carbon to climate change constrained by carbon dioxide variability. *Nature*, *494*(7437), 341–344. https://doi.org/10.1038/nature11882

Destouni, G., Jaramillo, F., & Prieto, C. (2013). Hydroclimatic shifts driven by human water use for food and energy production. *Nature Climate Change*, *3*(3), 213–217. https://doi.org/10.1038/nclimate1719

Dirmeyer, P. A., & Zeng, F. J. (1999). Precipitation Infiltration in the Simplified SiB Land Surface Scheme. *Journal of the Meteorological Society of Japan. Ser. II*, *77*(1B), 291–303. https://doi.org/10.2151/jmsj1965.77.1B_291

Dirmeyer, P. A., Jin, Y., Singh, B., & Yan, X. (2013a). Evolving Land–Atmosphere Interactions over North America from CMIP5 Simulations. *Journal of Climate*, *26*(19), 7313–7327. https://doi.org/10.1175/JCLI-D-12-00454.1

Dirmeyer, P. A., Jin, Y., Singh, B., & Yan, X. (2013b). Trends in Land–Atmosphere Interactions from CMIP5 Simulations. *Journal of Hydrometeorology*, *14*(3), 829–849. https://doi.org/10.1175/JHM-D-12-0107.1

Donohue, R. J., Roderick, M. L., & McVicar, T. R. (2012). Roots, storms and soil pores: Incorporating key ecohydrological processes into Budyko's hydrological model. *Journal of Hydrology*, *436–437*, 35–50. https://doi.org/10.1016/j.jhydrol.2012.02.033

Eyring, V., Bony, S., Meehl, G. A., Senior, C. A., Stevens, B., Stouffer, R. J., & Taylor, K. E. (2016). Overview of the Coupled Model Intercomparison Project Phase 6 (CMIP6) experimental design and organization. *Geoscientific Model Development*, *9*(5), 1937–1958. https://doi.org/10.5194/gmd-9-1937-2016

Fisher, R. A., Koven, C. D., Anderegg, W. R. L., Christoffersen, B. O., Dietze, M. C., Farrior, C. E., et al. (2018). Vegetation demographics in Earth System Models: A review of progress and priorities. *Global Change Biology*, *24*(1), 35–54. https://doi.org/10.1111/gcb.13910

Greve, P., Burek, P., & Wada, Y. (2020). Using the Budyko Framework for Calibrating a Global Hydrological Model. *Water Resources Research*, *56*(6), e2019WR026280. https://doi.org/10.1029/2019WR026280

He, Y., Peng, S., Liu, Y., Li, X., Wang, K., Ciais, P., et al. (2020). Global vegetation biomass production efficiency constrained by models and observations. *Global Change Biology*, *26*(3), 1474–1484. https://doi.org/10.1111/gcb.14816

Hurk, B. van den, Kim, H., Krinner, G., Seneviratne, S. I., Derksen, C., Oki, T., et al. (2016). LS3MIP (v1.0) contribution to CMIP6: the Land Surface, Snow and Soil moisture Model Intercomparison Project – aims, setup and expected outcome. *Geoscientific Model Development*, *9*(8), 2809–2832. https://doi.org/10.5194/gmd-9-2809-2016

Jiang, C., Xiong, L., Wang, D., Liu, P., Guo, S., & Xu, C.-Y. (2015). Separating the impacts of climate change and human activities on runoff using the Budyko-type equations with time-varying parameters. *Journal of Hydrology*, *522*, 326–338. https://doi.org/10.1016/j.jhydrol.2014.12.060

Koster, R. (2015). "Efficiency Space": A Framework for Evaluating Joint Evaporation and Runoff Behavior*. *Bulletin of the American Meteorological Society*, *96*(3), 393–396. https://doi.org/10.1175/BAMS-D-14-00056.1

Koster, R. D., & Suarez, M. J. (1999). A Simple Framework for Examining the Interannual Variability of Land Surface Moisture Fluxes. *Journal of Climate*, *12*(7), 1911–1917. https://doi.org/10.1175/1520-0442(1999)012<1911:ASFFET>2.0.CO;2

Kumar, S., Zwiers, F., Dirmeyer, P. A., Lawrence, D. M., Shrestha, R., & Werner, A. T. (2016). Terrestrial contribution to the heterogeneity in hydrological changes under global warming. *Water Resources Research*, *52*(4), 3127–3142. https://doi.org/10.1002/2016WR018607

Lawrence, D. M., Hurtt, G. C., Arneth, A., Brovkin, V., Calvin, K. V., Jones, A. D., et al. (2016). The Land Use Model Intercomparison Project (LUMIP) contribution to CMIP6: rationale and experimental design. *Geoscientific Model Development*, *9*(9), 2973–2998. https://doi.org/10.5194/gmd-9-2973-2016

Li, L., Wang, Y., Arora, V. K., Eamus, D., Shi, H., Li, J., et al. (2018). Evaluating Global Land Surface Models in CMIP5: Analysis of Ecosystem Water- and Light-Use Efficiencies and Rainfall Partitioning. *Journal of Climate*, *31*(8), 2995–3008. https://doi.org/10.1175/JCLI-D-16-0177.1

Lian, X., Piao, S., Huntingford, C., Li, Y., Zeng, Z., Wang, X., et al. (2018). Partitioning global land evapotranspiration using CMIP5 models constrained by observations. *Nature Climate Change*, *8*(7), 640–646. https://doi.org/10.1038/s41558-018-0207-9

Milly, P. C. D. (1994). Climate, soil water storage, and the average annual water balance. *Water Resources Research*, *30*(7), 2143–2156. https://doi.org/10.1029/94WR00586

Milly, P. C. D., & Dunne, K. A. (2016). Potential evapotranspiration and continental drying. *Nature Climate Change*, *6*(10), 946–949. https://doi.org/10.1038/nclimate3046

Milly, P. C. D., Betancourt, J., Falkenmark, M., Hirsch, R. M., Kundzewicz, Z. W., Lettenmaier, D. P., & Stouffer, R. J. (2008). Stationarity Is Dead: Whither Water Management? *Science*, *319*(5863), 573–574. https://doi.org/10.1126/science.1151915

Milly, P. C. D., Betancourt, J., Falkenmark, M., Hirsch, R. M., Kundzewicz, Z. W., Lettenmaier, D. P., et al. (2015). On Critiques of "Stationarity is Dead: Whither Water Management?" *Water Resources Research*, *51*(9), 7785–7789. https://doi.org/10.1002/2015WR017408

Miralles, D. G., Jiménez, C., Jung, M., Michel, D., Ershadi, A., McCabe, M. F., et al. (2016). The WACMOS-ET project – Part 2: Evaluation of global terrestrial evaporation data sets. *Hydrology and Earth System Sciences*, *20*(2), 823–842. https://doi.org/10.5194/hess-20-823-2016

Ning, T., Zhou, S., Chang, F., Shen, H., Li, Z., & Liu, W. (2019). Interaction of vegetation, climate and topography on evapotranspiration modelling at different time scales within the Budyko framework. *Agricultural and Forest Meteorology*, *275*, 59–68. https://doi.org/10.1016/j.agrformet.2019.05.001

Osborne, J. M., & Lambert, F. H. (2018). A simple tool for refining GCM water availability projections, applied to Chinese catchments. *Hydrology and Earth System Sciences*, *22*(11), 6043–6057. https://doi.org/10.5194/hess-22-6043-2018

Oudin, L., Andréassian, V., Lerat, J., & Michel, C. (2008). Has land cover a significant impact on mean annual streamflow? An international assessment using 1508 catchments. *Journal of Hydrology*, *357*(3), 303–316. https://doi.org/10.1016/j.jhydrol.2008.05.021

Porada, P., Kleidon, A., & Schymanski, S. J. (2011). Entropy production of soil hydrological processes and its maximisation. *Earth System Dynamics*, *2*(2), 179–190. https://doi.org/10.5194/esd-2-179-2011

Roderick, M. L., & Farquhar, G. D. (2011). A simple framework for relating variations in runoff to variations in climatic conditions and catchment properties. *Water Resources Research*, *47*(12). https://doi.org/10.1029/2010WR009826

Santanello, J. A., Dirmeyer, P. A., Ferguson, C. R., Findell, K. L., Tawfik, A. B., Berg, A., et al. (2018). Land-Atmosphere Interactions: The LoCo Perspective. *Bulletin of the American Meteorological Society*, *99*, 1253–1272. https://doi.org/10.1175/BAMS-D-17-0001.1

Singh, R., & Kumar, R. (2015). Vulnerability of water availability in India due to climate change: A bottom-up probabilistic Budyko analysis. *Geophysical Research Letters*, *42*(22), 9799–9807. https://doi.org/10.1002/2015GL066363

Sposito, G. (2017). Understanding the Budyko Equation. *Water*, *9*(4), 236. https://doi.org/10.3390/w9040236

Taylor, K. E., Stouffer, R. J., & Meehl, G. A. (2012). An Overview of CMIP5 and the Experiment Design. *Bulletin of the American Meteorological Society*, *93*(4), 485–498. https://doi.org/10.1175/BAMS-D-11-00094.1

Wang, D., & Hejazi, M. (2011). Quantifying the relative contribution of the climate and direct human impacts on mean annual streamflow in the contiguous United States. *Water Resources Research*, *47*(10). https://doi.org/10.1029/2010WR010283

Wang, D., & Tang, Y. (2014). A one-parameter Budyko model for water balance captures emergent behavior in darwinian hydrologic models. *Geophysical Research Letters*, *41*(13), 4569–4577. https://doi.org/10.1002/2014GL060509

Wang, X., Zhao, C., Müller, C., Wang, C., Ciais, P., Janssens, I., et al. (2020). Emergent constraint on crop yield response to warmer temperature from field experiments. *Nature Sustainability*, *3*(11), 908–916. https://doi.org/10.1038/s41893-020-0569-7

Wu, D., Zhao, X., Liang, S., Zhou, T., Huang, K., Tang, B., & Zhao, W. (2015). Time-lag effects of global vegetation responses to climate change. *Global Change Biology*, *21*(9), 3520–3531. https://doi.org/10.1111/gcb.12945

Xu, X., Liu, W., Scanlon, B. R., Zhang, L., & Pan, M. (2013). Local and global factors controlling water-energy balances within the Budyko framework. *Geophysical Research Letters*, *40*(23), 6123–6129. https://doi.org/10.1002/2013GL058324

Yang, D., Shao, W., Yeh, P. J.-F., Yang, H., Kanae, S., & Oki, T. (2009). Impact of vegetation coverage on regional water balance in the nonhumid regions of China. *Water Resources Research*, *45*(7). https://doi.org/10.1029/2008WR006948

Yang, Hanbo, & Yang, D. (2011). Derivation of climate elasticity of runoff to assess the effects of climate change on annual runoff. *Water Resources Research*, *47*(7). https://doi.org/10.1029/2010WR009287

Yang, Hui, Piao, S., Huntingford, C., Ciais, P., Li, Y., Wang, T., et al. (2018). Changing the retention properties of catchments and their influence on runoff under climate change. *Environmental Research Letters*, *13*(9), 094019. https://doi.org/10.1088/1748-9326/aadd32

Ye, S., Li, H.-Y., Li, S., Leung, L. R., Demissie, Y., Ran, Q., & Blöschl, G. (2015). Vegetation regulation on streamflow intra-annual variability through adaption to climate variations. *Geophysical Research Letters*, *42*(23), 10,307-10,315. https://doi.org/10.1002/2015GL066396

Zhang, L., Dawes, W. R., & Walker, G. R. (2001). Response of mean annual evapotranspiration to vegetation changes at catchment scale. *Water Resources Research*, *37*(3), 701–708. https://doi.org/10.1029/2000WR900325

Zhang, L., Hickel, K., Dawes, W. R., Chiew, F. H. S., Western, A. W., & Briggs, P. R. (2004). A rational function approach for estimating mean annual evapotranspiration. *Water Resources Research*, *40*(2). https://doi.org/10.1029/2003WR002710

Zhang, S., Yang, H., Yang, D., & Jayawardena, A. W. (2016). Quantifying the effect of vegetation change on the regional water balance within the Budyko framework. *Geophysical Research Letters*, *43*(3), 1140–1148. https://doi.org/10.1002/2015GL066952

Zhang, S., Yang, Y., McVicar, T. R., & Yang, D. (2018). An Analytical Solution for the Impact of Vegetation Changes on Hydrological Partitioning Within the Budyko Framework. *Water Resources Research*, *54*(1), 519–537. https://doi.org/10.1002/2017WR022028

Zheng, H., Chiew, F. H. S., Charles, S., & Podger, G. (2018). Future climate and runoff projections across South Asia from CMIP5 global climate models and hydrological modelling. *Journal of Hydrology: Regional Studies*, *18*, 92–109. https://doi.org/10.1016/j.ejrh.2018.06.004

Zhou, G., Wei, X., Chen, X., Zhou, P., Liu, X., Xiao, Y., et al. (2015). Global pattern for the effect of climate and land cover on water yield. *Nature Communications*, *6*(1), 5918. https://doi.org/10.1038/ncomms6918

Table 1. List of CMIP6 models used. Full citations for each model are included in the supplement. "Grid" is for the atmospheric model component (horizontal cells: longitude x latitude).

Institution	CMIP Label	Version	Variant	Grid	DOI
AWI	AWI-CM-1-1-MR	20191015	r1i1p1f1	384x192	10.22033/ESGF/CMIP6.359
BCC	BCC-CSM2-MR	20181015	r1i1p1f1	320x160	10.22033/ESGF/CMIP6.1725
BCC	BCC-ESM1	20190613	r1i1p1f1	128x64	10.22033/ESGF/CMIP6.1734
CAMS	CAMS-CSM1-0	20190708	r1i1p1f1	320x160	10.22033/ESGF/CMIP6.1399
CCCma	CanESM5	20190429	r1i1p1f1	128x64	10.22033/ESGF/CMIP6.1303
NCAR	CESM2	20190425	r1i1p1f1	288x192	10.22033/ESGF/CMIP6.2185
NCAR	CESM2-WACCM	20190425	r1i1p1f1	288x192	10.22033/ESGF/CMIP6.10024
NCAR	CESM2-WACCM-FV2	20200226	r1i1p1f1	144x96	10.22033/ESGF/CMIP6.11282
CNRM-CERFACS	CNRM-CM6-1	20180626	r1i1p1f2	256x128	10.22033/ESGF/CMIP6.1375
CNRM-CERFACS	CNRM-ESM2-1	20181018	r1i1p1f2	256x128	10.22033/ESGF/CMIP6.1391
E3SM-Project	E3SM-1-0	20190718	r1i1p1f1	360x180	10.22033/ESGF/CMIP6.2294
EC-Earth-Consortium	EC-Earth3	20200727	r1i1p1f1**	512x256	10.22033/ESGF/CMIP6.181
EC-Earth-Consortium	EC-Earth3-Veg	20200325	r1i1p1f1	512x256	10.22033/ESGF/CMIP6.642
CAS	FGOALS-g3	20191215	r1i1p1f1	180x80	10.22033/ESGF/CMIP6.1783
GFDL	GFDL-CM4	20180701	r1i1p1f1	288x180	10.22033/ESGF/CMIP6.1402
GFDL	GFDL-ESM4	20180701	r1i1p1f1	288x180	10.22033/ESGF/CMIP6.1407
NASA-GISS	GISS-E2-1-G	20180905	r1i1p1f1	144x90	10.22033/ESGF/CMIP6.1400
NASA-GISS	GISS-E2-1-H	20190403	r1i1p1f1	144x90	10.22033/ESGF/CMIP6.1421
MOHC	HadGEM3-GC31-LL	20190620	r1i1p1f3*	192x144	10.22033/ESGF/CMIP6.419
MOHC	HadGEM3-GC31-MM	20200115	r1i1p1f3*	432x324	10.22033/ESGF/CMIP6.420
INM	INM-CM4-8	20200226	r1i1p1f1	180x120	10.22033/ESGF/CMIP6.1422
INM	INM-CM5-0	20190530	r1i1p1f1	180x120	10.22033/ESGF/CMIP6.1423
IPSL	IPSL-CM6A-LR	20180727	r1i1p1f1	144x143	10.22033/ESGF/CMIP6.13581
NIMS-KMA	KACE-1-0-G	20190916	r1i1p1f1	192x144	10.22033/ESGF/CMIP6.2241
U. Arizona	MCM-UA-1-0	20190731	r1i1p1f1	96x80	10.22033/ESGF/CMIP6.2421
MIROC	MIROC-ES2L	20190823	r1i1p1f2	128x64	10.22033/ESGF/CMIP6.902
MIROC	MIROC6	20181212	r1i1p1f1	256x128	10.22033/ESGF/CMIP6.9121
HAMMOZ-Consortium	MPI-ESM-1-2-HAM	20190628	r1i1p1f1	192x96	10.22033/ESGF/CMIP6.1622
MPI-M DWD DKRZ	MPI-ESM1-2-HR	20190710	r1i1p1f1	384x192	10.22033/ESGF/CMIP6.741
MPI-M AWI	MPI-ESM1-2-LR	20190710	r1i1p1f1	192x96	10.22033/ESGF/CMIP6.742
MRI	MRI-ESM2-0	20190308	r1i1p1f1	320x160	10.22033/ESGF/CMIP6.621
NUIST	NESM3	20190707	r1i1p1f1	192x96	10.22033/ESGF/CMIP6.2021
NCC	NorCPM1	20190914	r1i1p1f1	144x96	10.22033/ESGF/CMIP6.10843
NCC	NorESM2-LM	20190815	r1i1p1f1	144x96	10.22033/ESGF/CMIP6.502
SNU	SAM0-UNICON	20190323	r1i1p1f1	288x192	10.22033/ESGF/CMIP6.1489
AS-RCEC	TaiESM1	20200225	r1i1p1f1	288x192	10.22033/ESGF/CMIP6.9684
MOHC NERC NIMS-KMA NIWA	UKESM1-0-LL	20190406	r1i1p1f2	192x144	10.22033/ESGF/CMIP6.1569

* piControl alone is r1i1p1f1 ** r3i1p1f1 for 1pctCO2 and r8i1p1f1 for 4xCO2

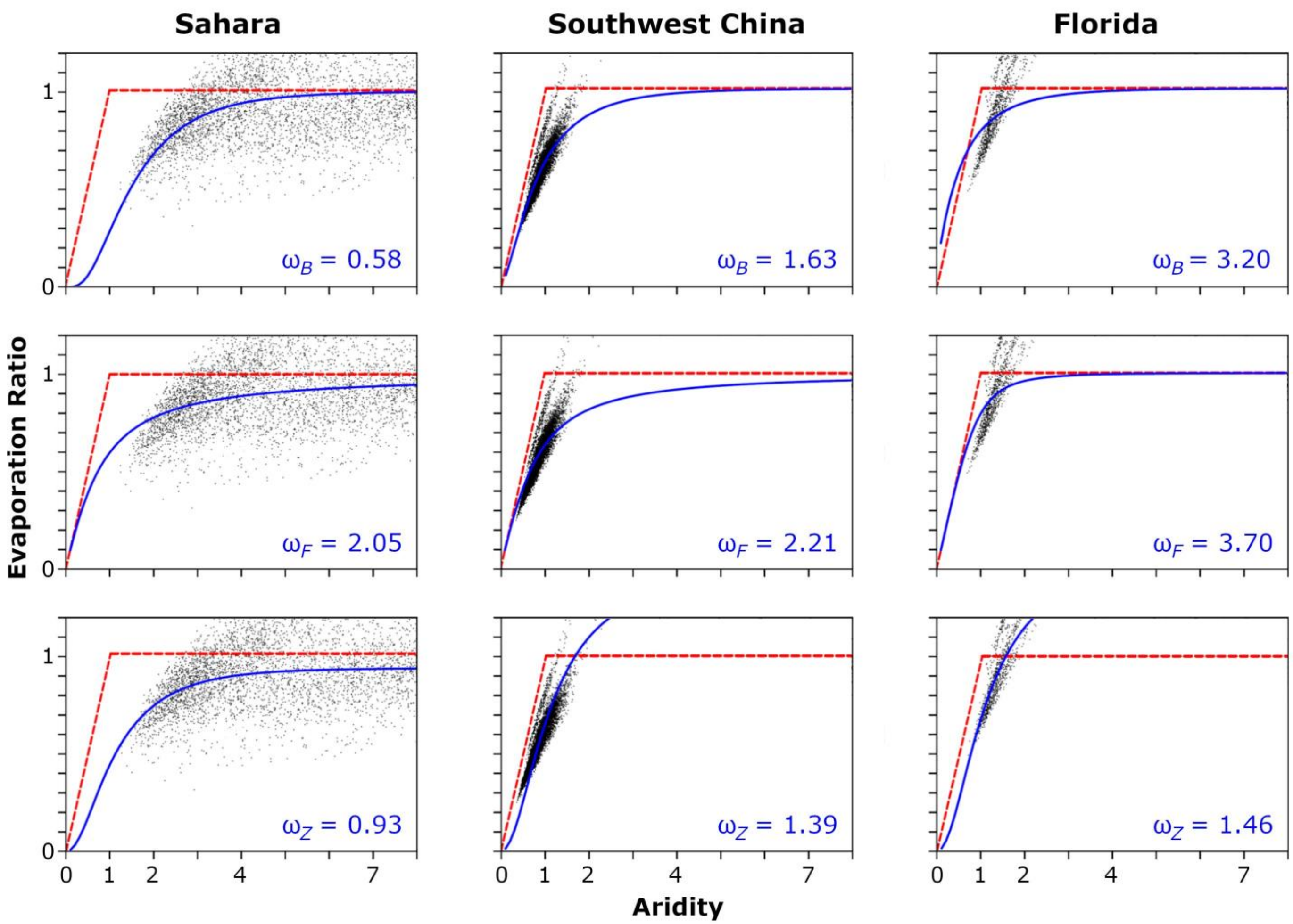

Figure 1. Comparison of the best fits (blue curves) through yearly data from a piControl simulation of a CMIP6 model at three different locations (labeled columns) for three formulations of the Budyko curve. Top row: Budyko formulation with tunable exponent; middle row: Fu (1981) formulation; bottom row: Budyko formulation without E/P constraint. Values of the single tunable exponent are shown in each panel, as are the theoretical energy and water limits (dashed red lines). Units of the axes are dimensionless.

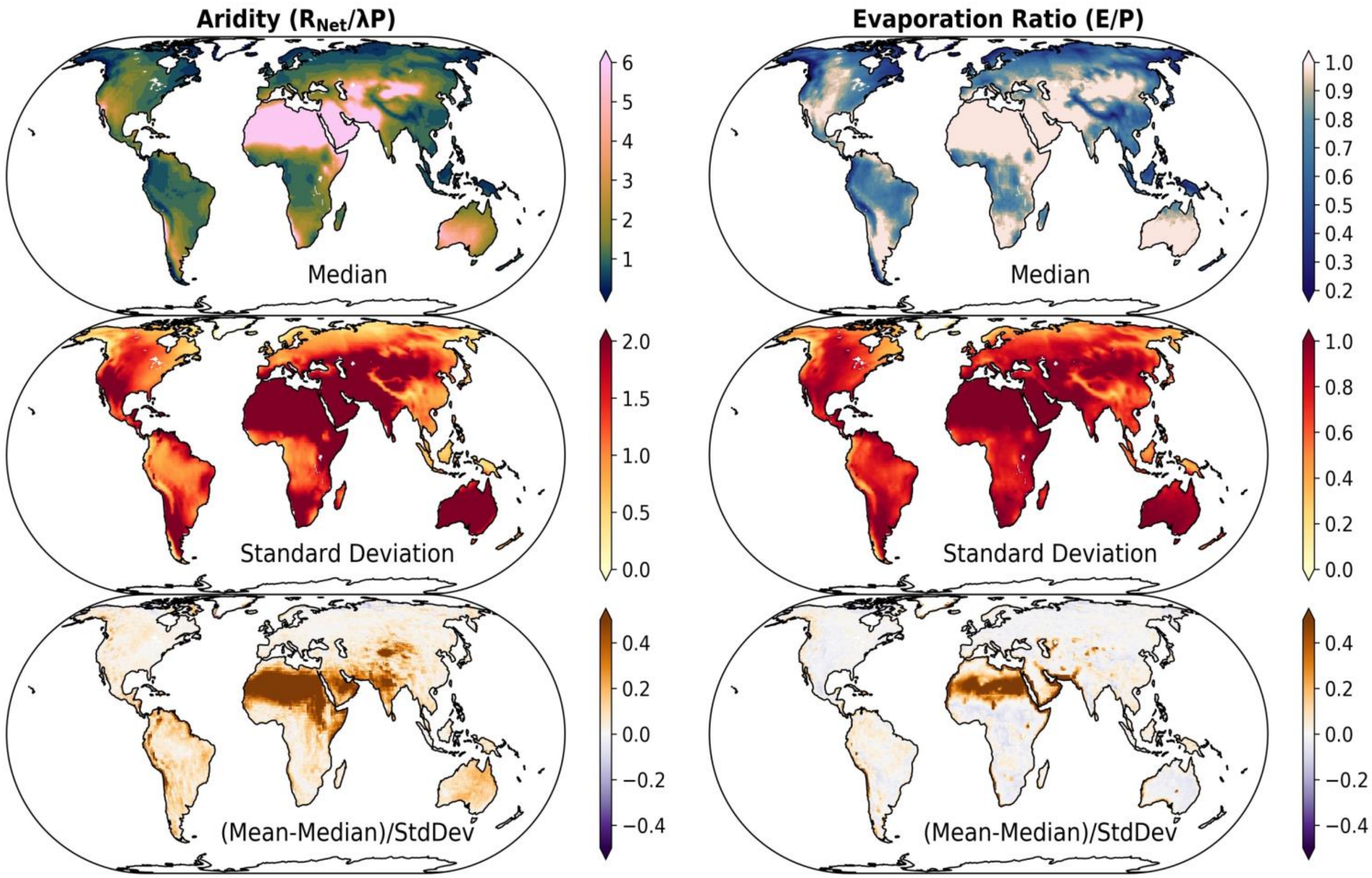

Figure 2. Multi-model statistics of aridity (left column) and E ratio (right column) calculated from each model's time-median from the piControl simulation. Top row: median at each location of individual model time-medians; middle row: standard deviation at each location of individual model time-medians; bottom row: The difference between the mean and median of individual model time-medians normalized by the standard deviation of individual model time-medians. All units are dimensionless.

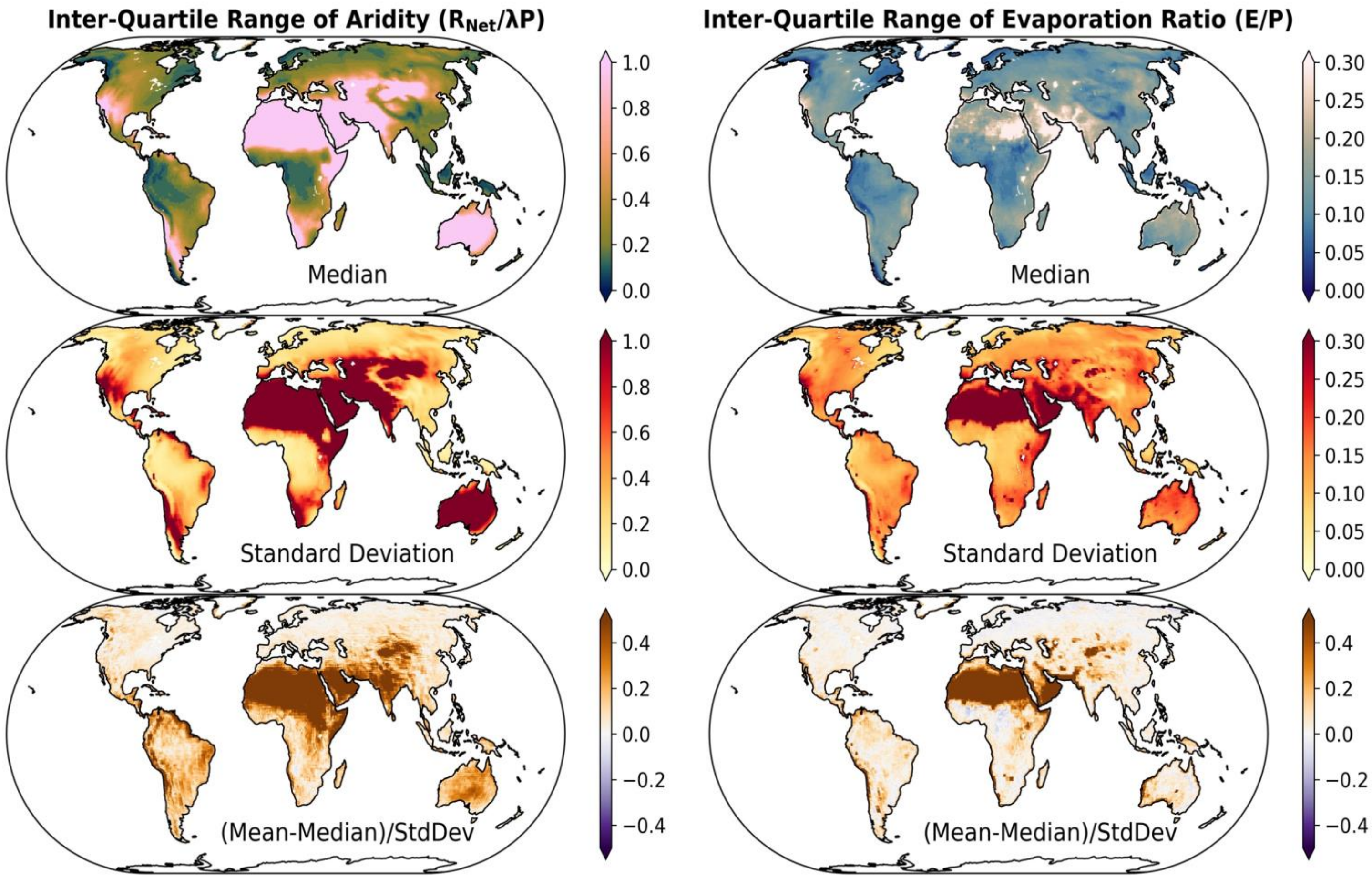

Figure 3. As in Figure 2 but applied to each model's inter-quartile ranges across all piControl years instead of each model's time medians.

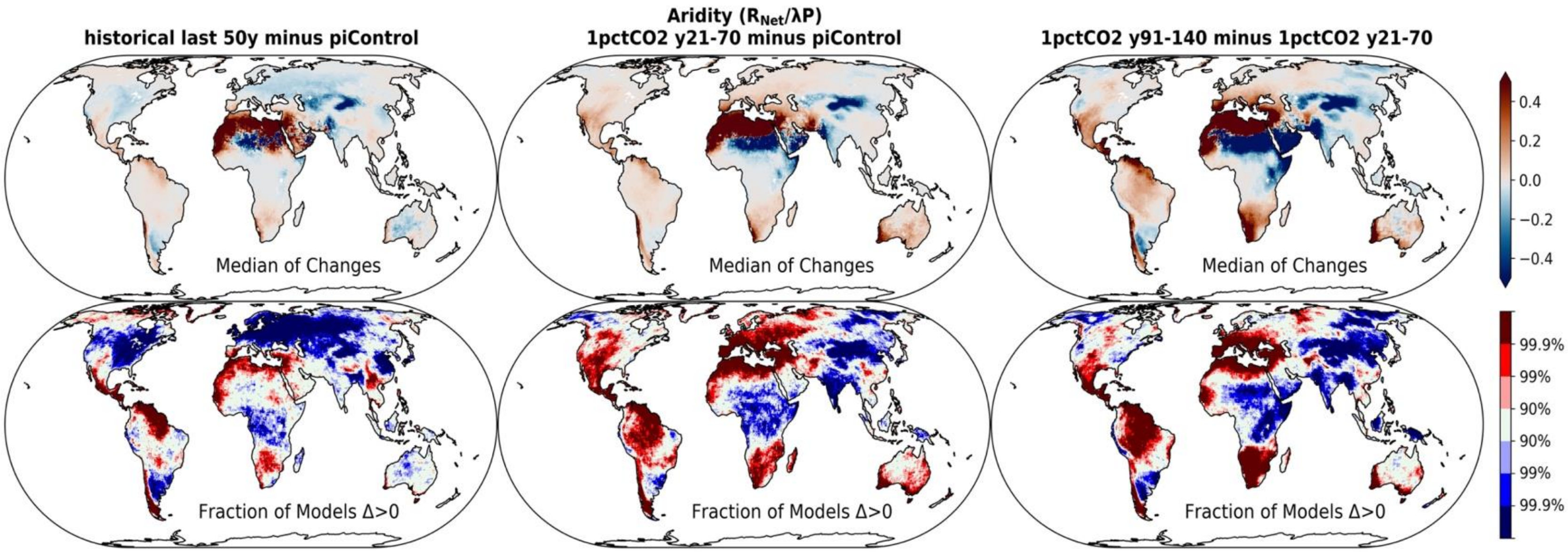

Figure 4. Changes in aridity from PI to H_{L50} (left column); PI to $1\%_{21\text{-}70}$ (middle column); $1\%_{21\text{-}70}$ to $1\%_{91\text{-}140}$ (right column). The top row shows the median change across all models at each location. The bottom row shows the significance of the fraction of models agreeing on the sign of the change (red for positive change, blue for negative change).

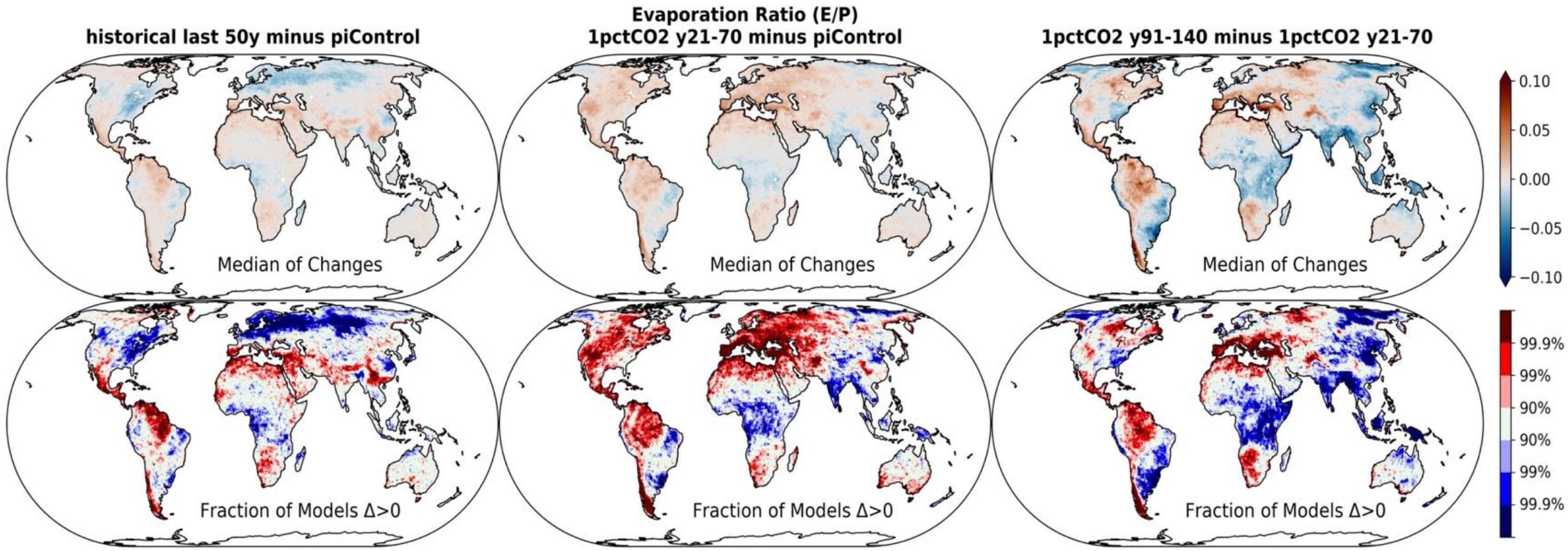

Figure 5. As in Figure 4 for E ratio.

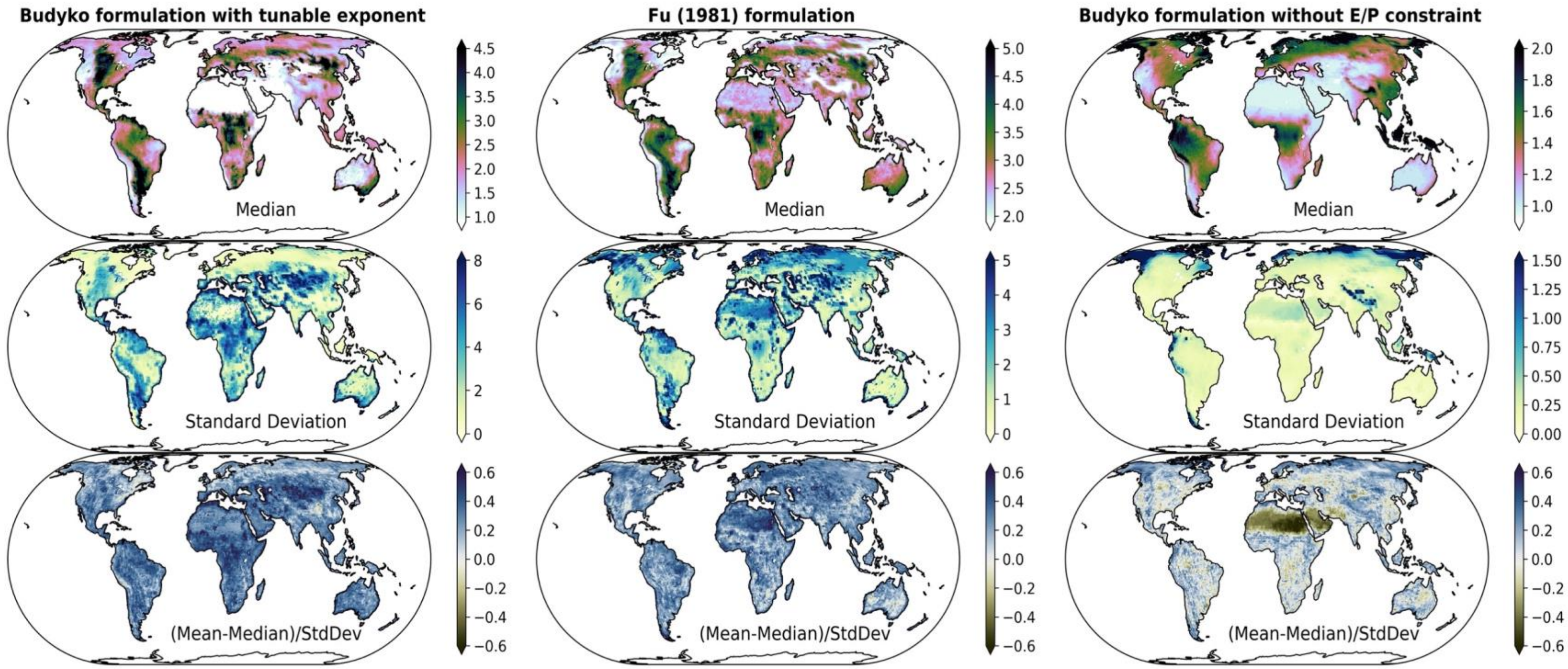

Figure 6. As in Figure 2 but for the single parameter of the indicated formulations: ω_B (left column); ω_F (middle column); ω_Z (right column).

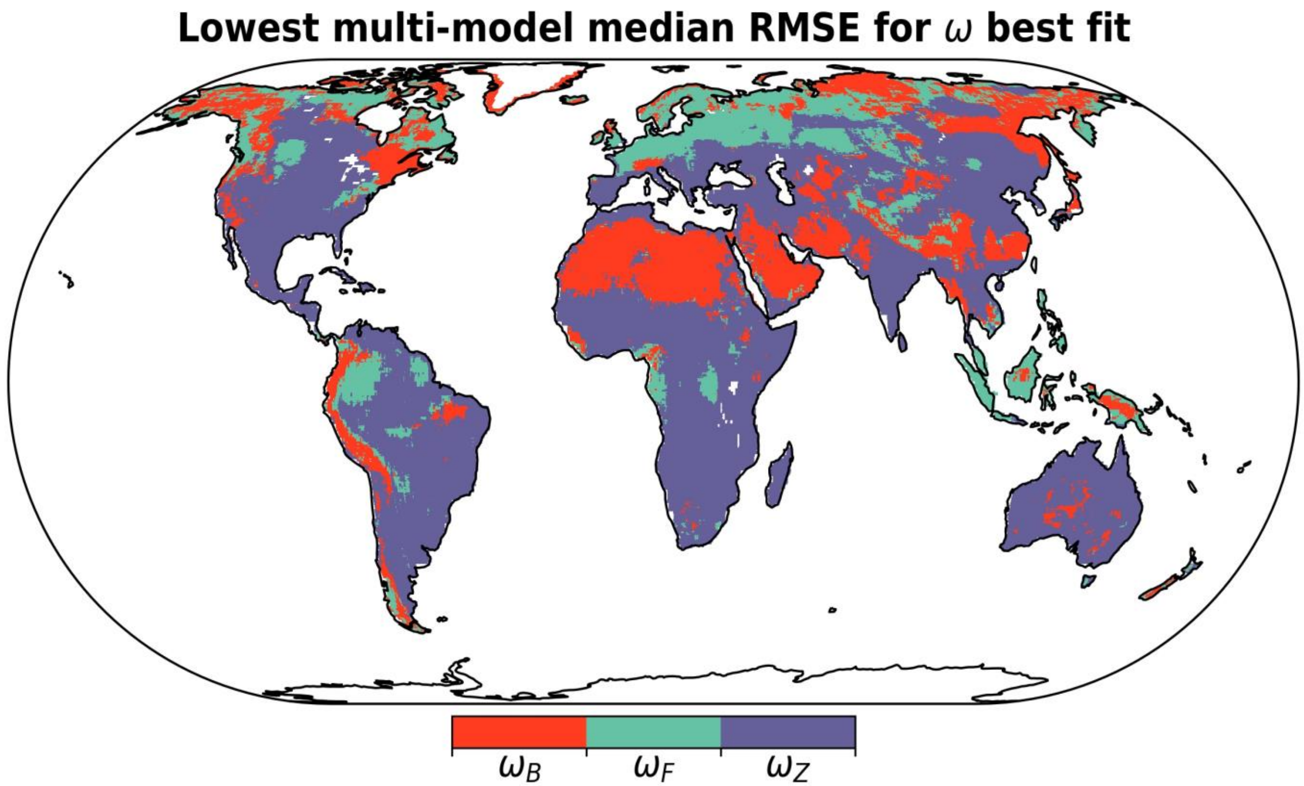

Figure 7. Colors indicate which formulation of the Budyko curve best fits the distribution of annual values of E/P and $R_{net}/\lambda P$ across all models for the piControl experiment: ω_B indicates the Budyko formulation with the tunable exponent, ω_F is the Fu (1981) formulation, and ω_Z is the Budyko formulation without the E/P constraint.

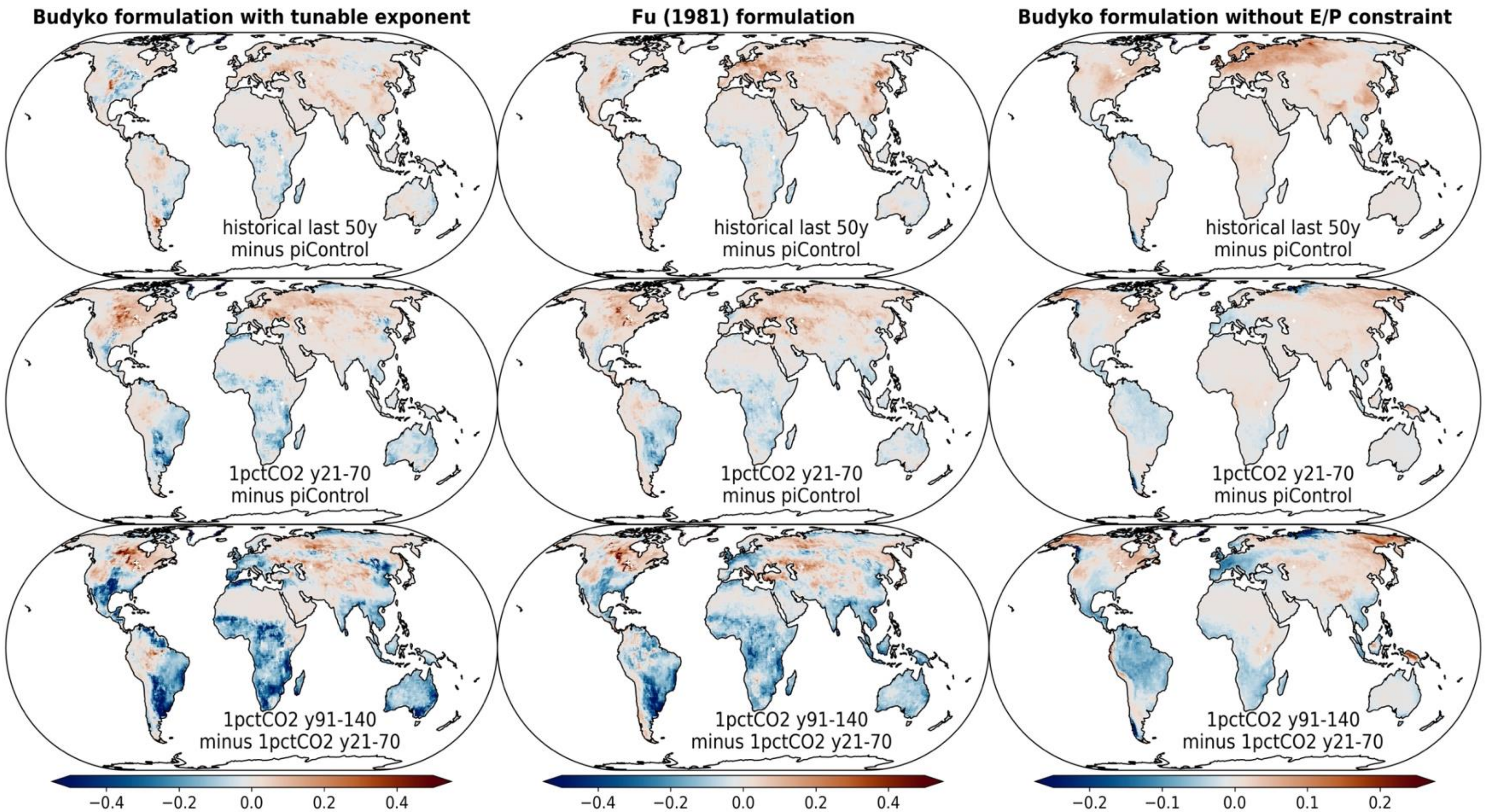

842
843 **Figure 8**. Changes from PI to H_{L50} (top row); PI to $1\%_{21\text{-}70}$ (middle row); $1\%_{21\text{-}70}$ to $1\%_{91\text{-}140}$ (bottom row) for the single parameter of
844 the indicated formulations: ω_B (left column); ω_F (middle column); ω_Z (right column).
845
846
847

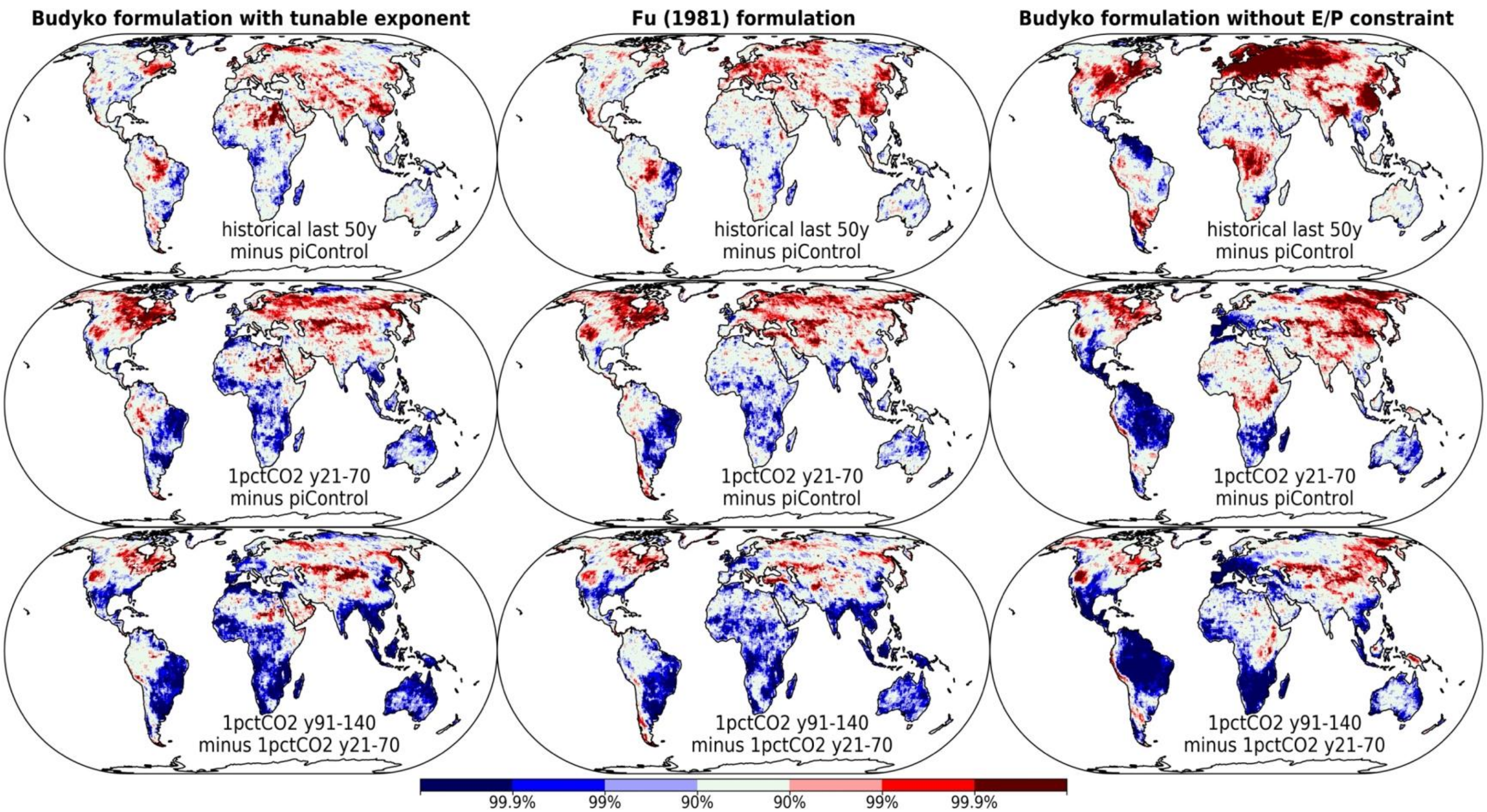

Figure 9. As in Figure 8 for the significance of the fraction of models agreeing on the sign of the change in ω (red for positive changes, blue for negative changes).

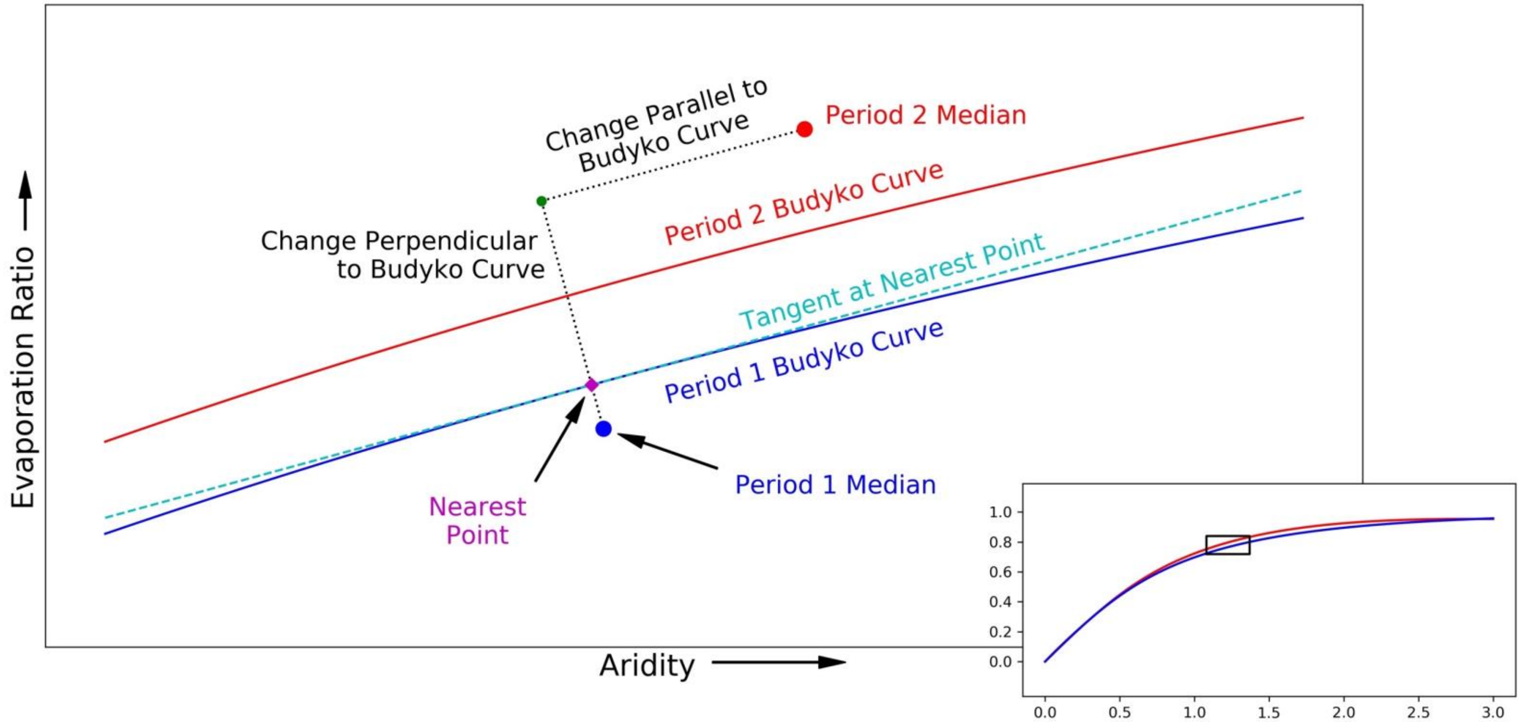

Figure 10. Schematic showing two Budyko curves (blue and red) representing choices of ω that best fit the scatter of annual values of aridity and E ratio at a grid cell for two different periods in DECK simulations, or between PI and H_{L50} simulations. The main panel zooms in on the box indicated in the inset. The multi-model median values of aridity and E ratio for the different periods are shown by the large dots, and the best fit curves in their neighborhood are shown by solid lines of matching color. For the earlier period (Period 1 in blue), the nearest point on the Budyko curve to the median values is shown as a purple diamond. The slope of that curve is used to rotate the coordinate system to project the difference to median in the later period (Period 2 in red) into perpendicular and parallel components.

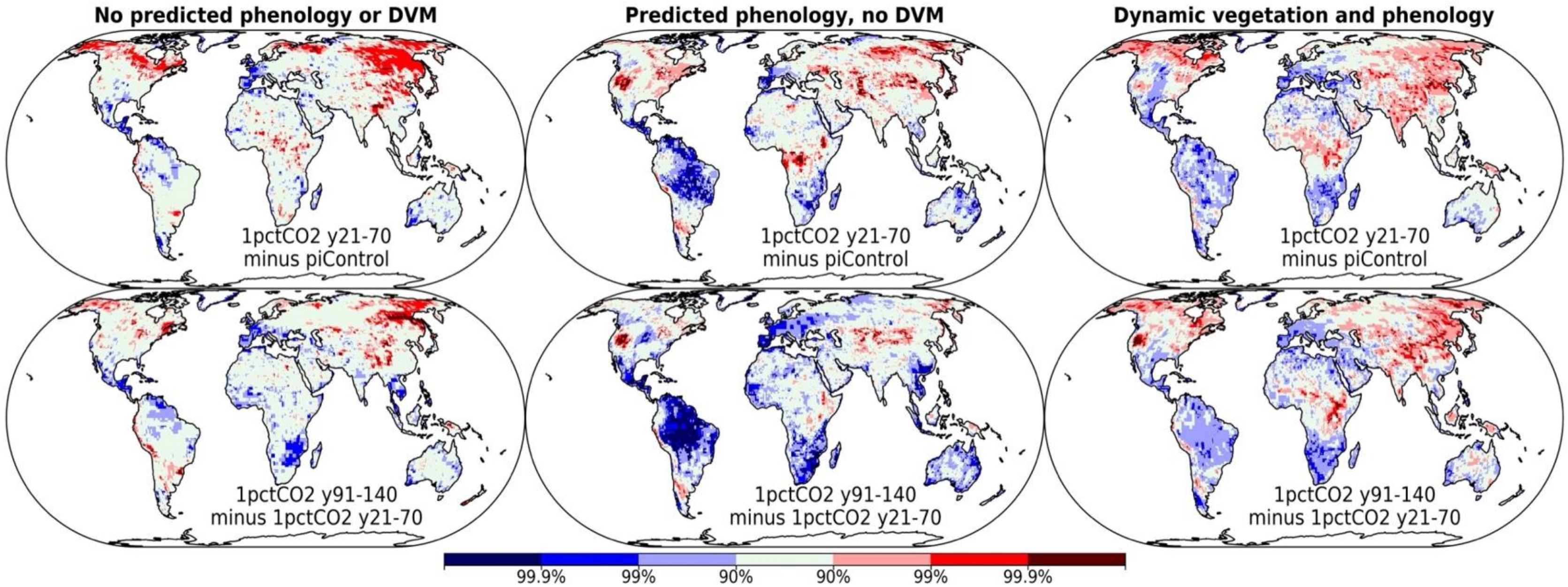

Figure 11. Significance of model agreement in the changes in ω_Z from PI to $1\%_{21\text{-}70}$ (top row) and $1\%_{21\text{-}70}$ to $1\%_{91\text{-}140}$ (bottom row) only for models without predicted vegetation phenology or dynamic vegetation (left column), with predicted phenology but no dynamic vegetation (middle column) and with both dynamic vegetation and predicted phenology (right column).

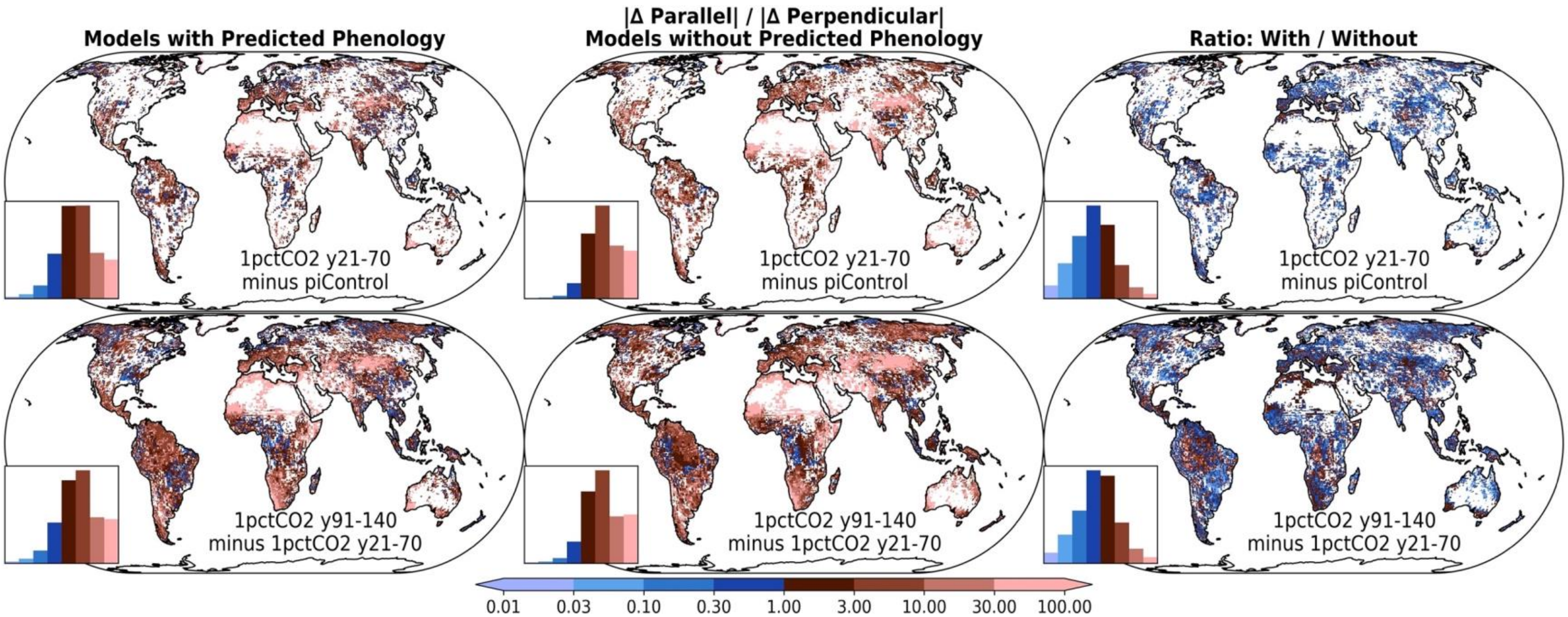

Figure 12. The ratio of change parallel to the Budyko curve to change perpendicular to the Budyko curve from PI to $1\%_{21\text{-}70}$ (top row) and $1\%_{21\text{-}70}$ to $1\%_{91\text{-}140}$ (bottom row) only for models with predicted phenology but no dynamic vegetation (left column) without predicted phenology or dynamic vegetation (middle column) and the ratio of values from the left column over the middle column (right column). The inset histogram with each panel shows the proportion of ice-free land area in each color band, indicated by the color bar at the bottom of the figure.

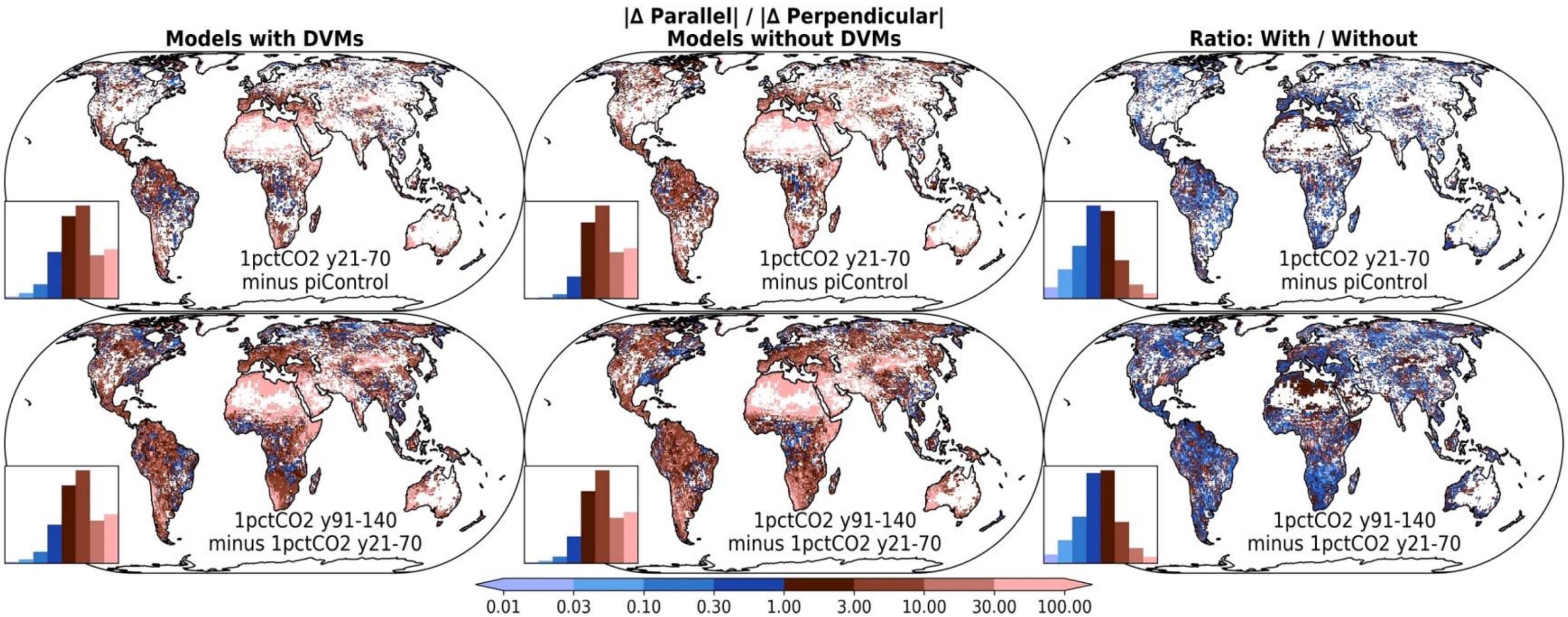

Figure 13. As in Figure 12, except the left column is only for models with both predicted phenology and dynamic vegetation, and the middle column is only for models with predicted phenology but no dynamic vegetation.

Earth's Future

Supporting Information for

Projected Hydroclimate Changes Driven by Carbon Dioxide Trends and Vegetation Modeling in CMIP6

Paul A. Dirmeyer[12], Kai Huang[2], Nikki Lydeen[2], Zachary Manthos[2], Scott Knapp[2] and Finley Miles Hay-Chapman[2]

[1]Center for Ocean-Land-Atmosphere Studies, George Mason University, Fairfax, Virginia, USA.

[2]Department of Atmospheric, Oceanic and Earth Sciences, George Mason University, Fairfax, Virginia, USA.

Contents of this file

Figures S1 to S8
Table S1

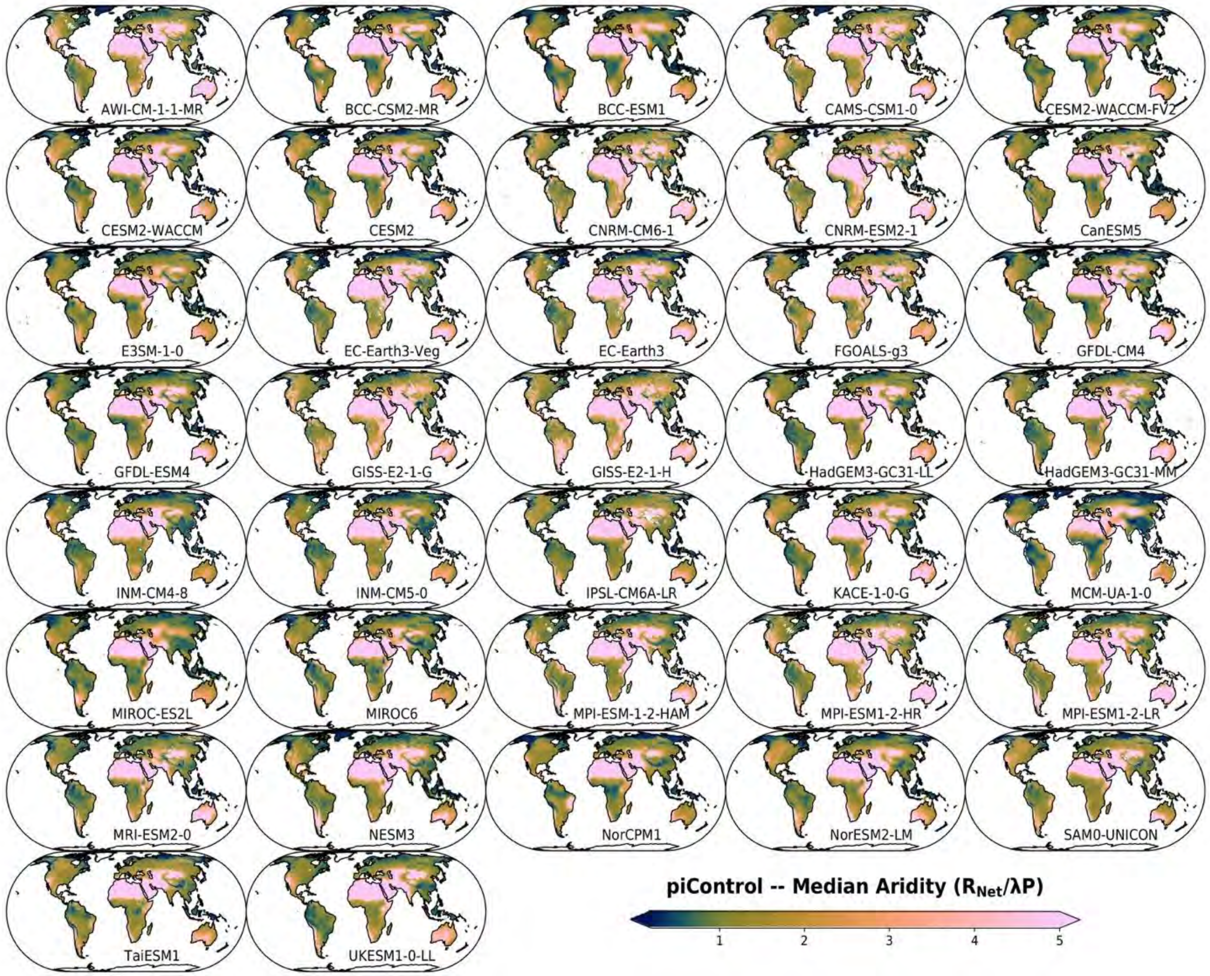

Figure S1. Time-median aridity values from the piControl simulation of each considered CMIP6 model.

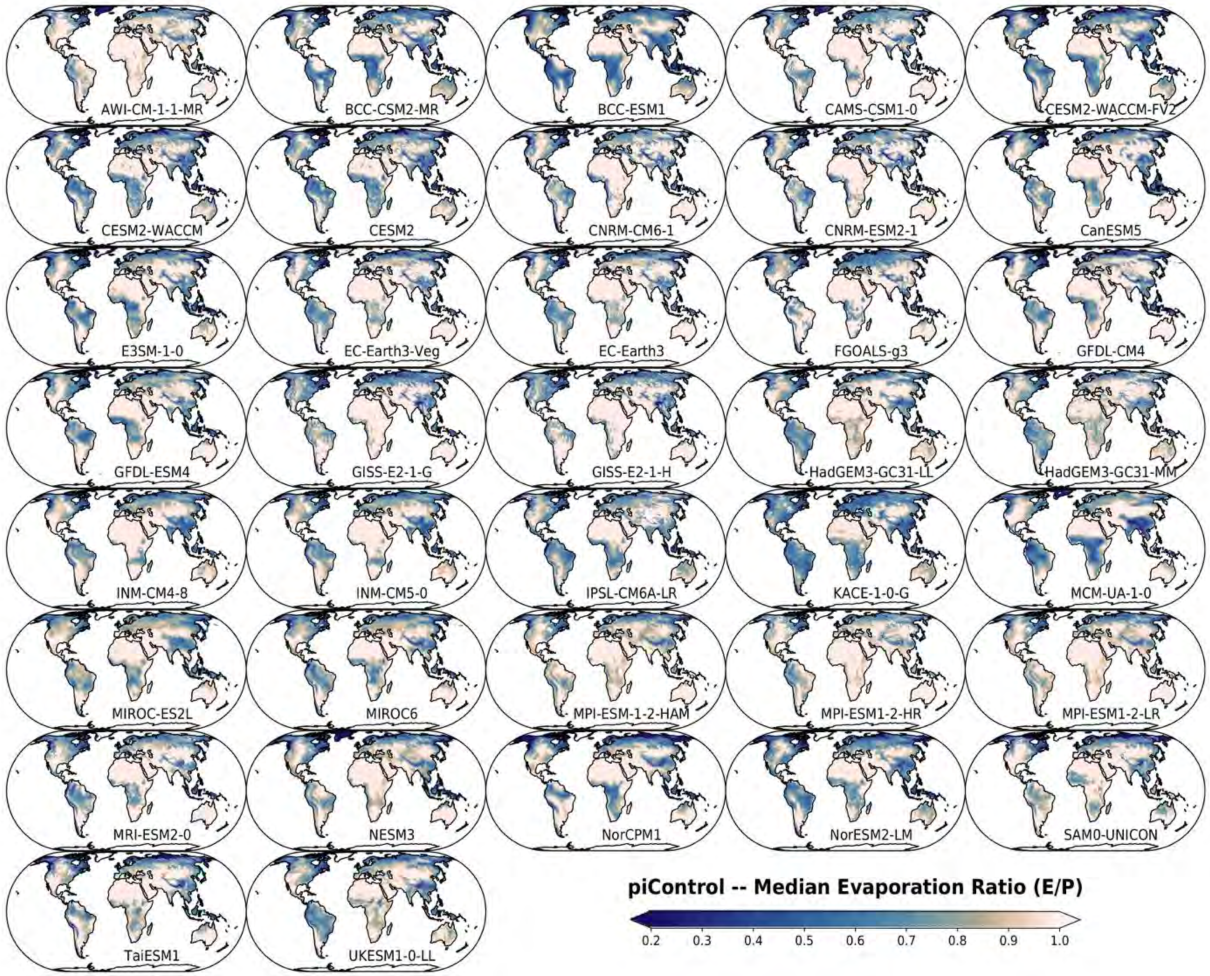

23 **Figure S2**. As in Figure S1 for E ratio.

24

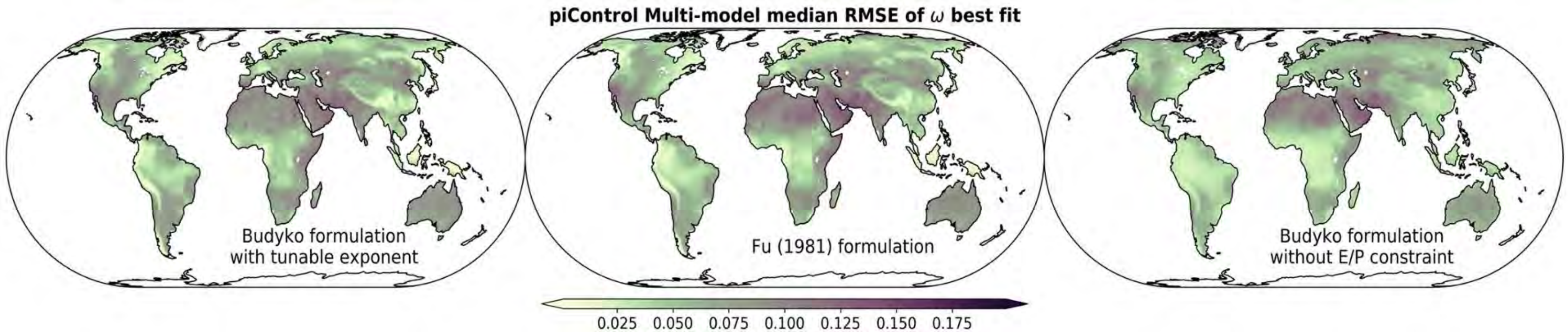

Figure S3. Root mean square error (RMSE) of the best fit Budyko curve of the indicated formulation through all yearly points in Budyko space (E/P versus $R_{net}/\lambda P$).

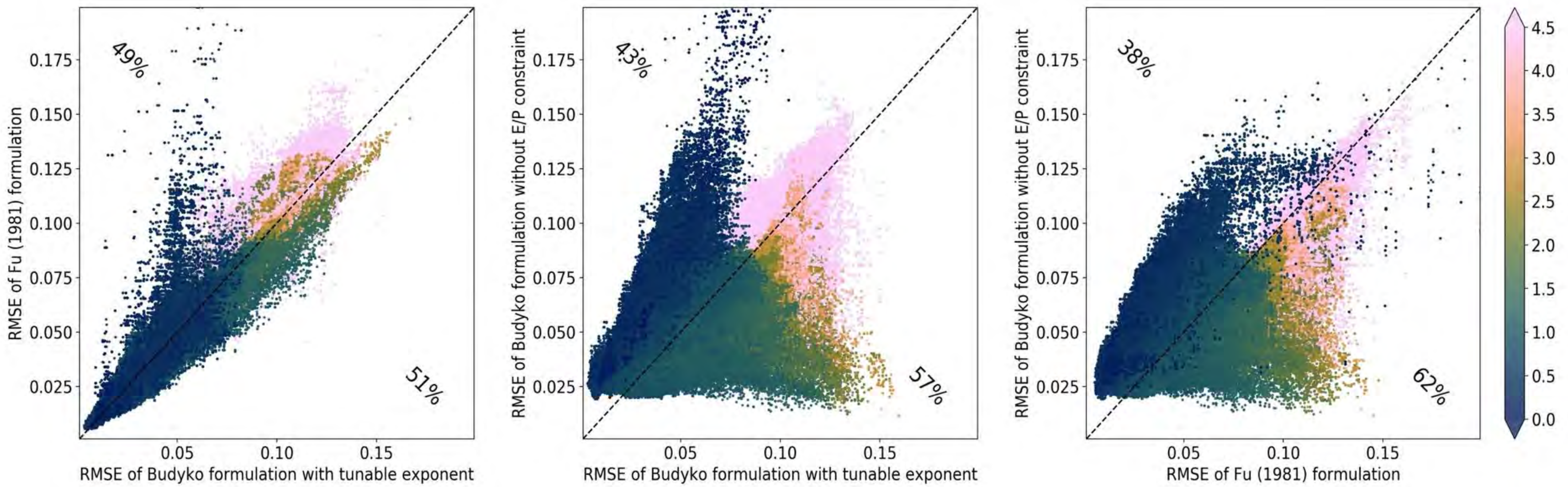

Figure S4. Scatter of multi-model median of RMSE of the optimal fit of the indicated Budyko formulation to the annual values of aridity and E ratio in the piControl experiment. Each point is a grid cell on the high-resolution interpolated grid. The percentages show the fraction of points on each side of the $x = y$ line. Coloring shows the multi-model median aridity calculated from each model's time-median at each grid cell.

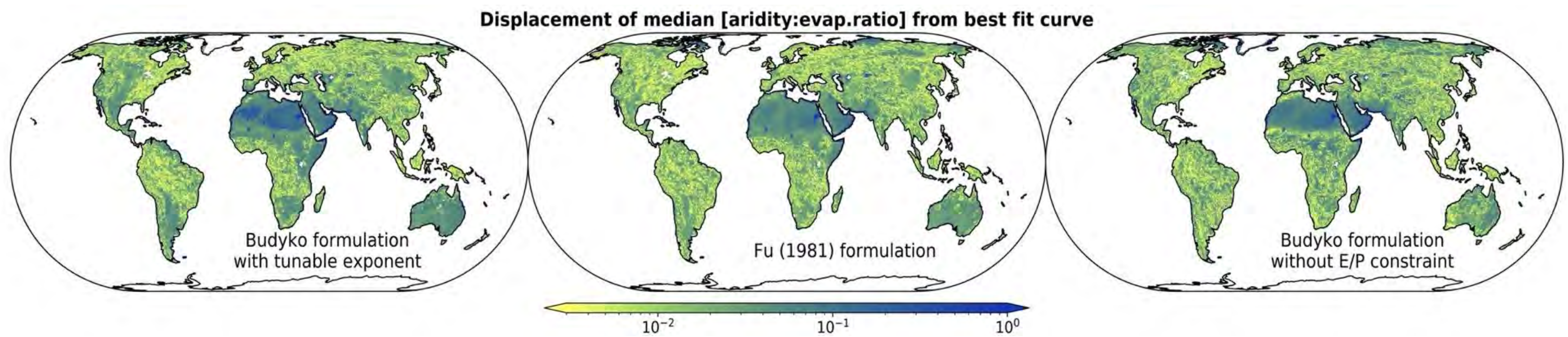

Figure S5. Displacement of the point in Budyko space representing the multi-model medians of aridity and E ratio from the nearest point on the best fit Budyko curve using the formulation indicated in each panel.

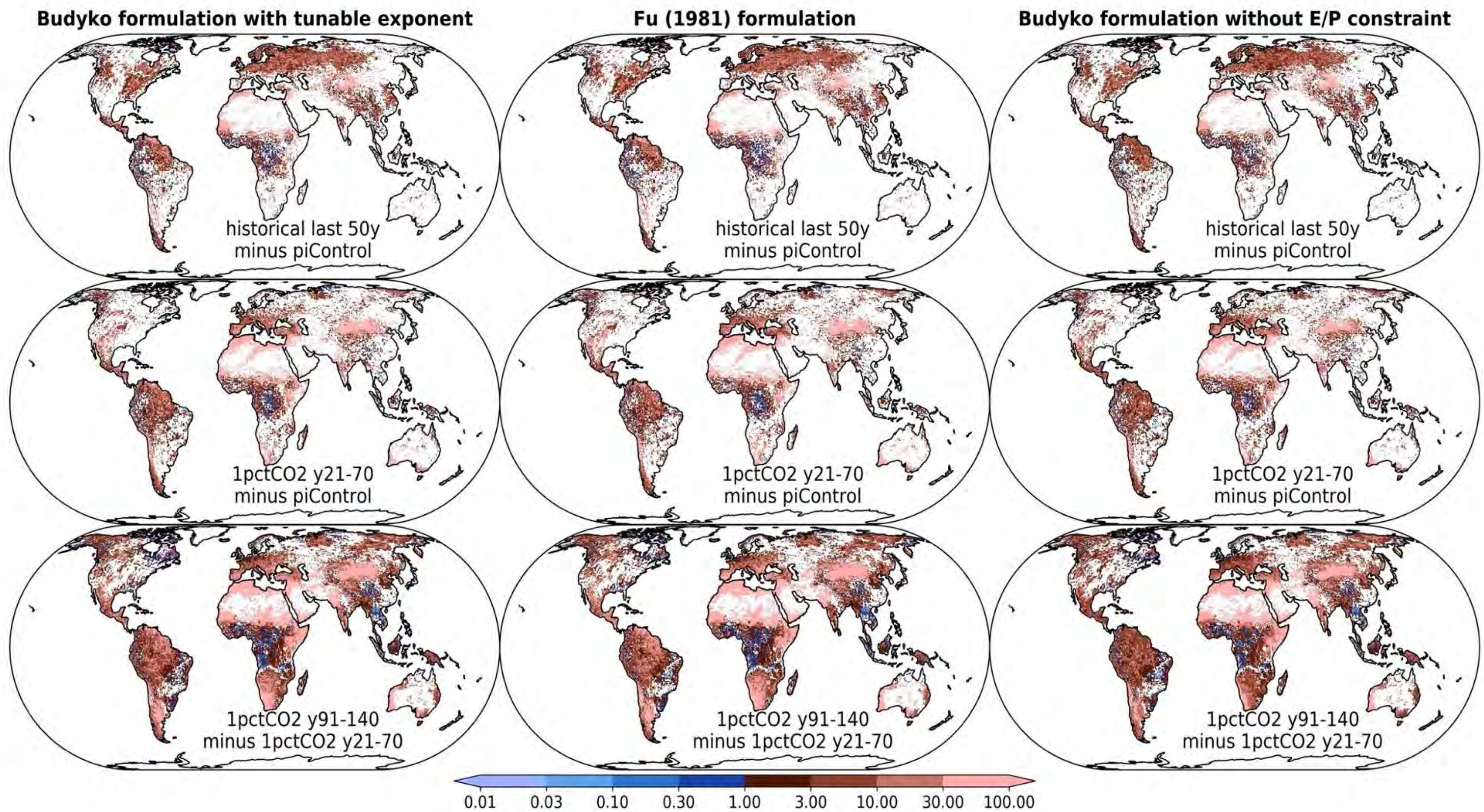

Figure S6. As in Figure 8 for the ratio of change parallel to the Budyko curve to change perpendicular to the Budyko curve.

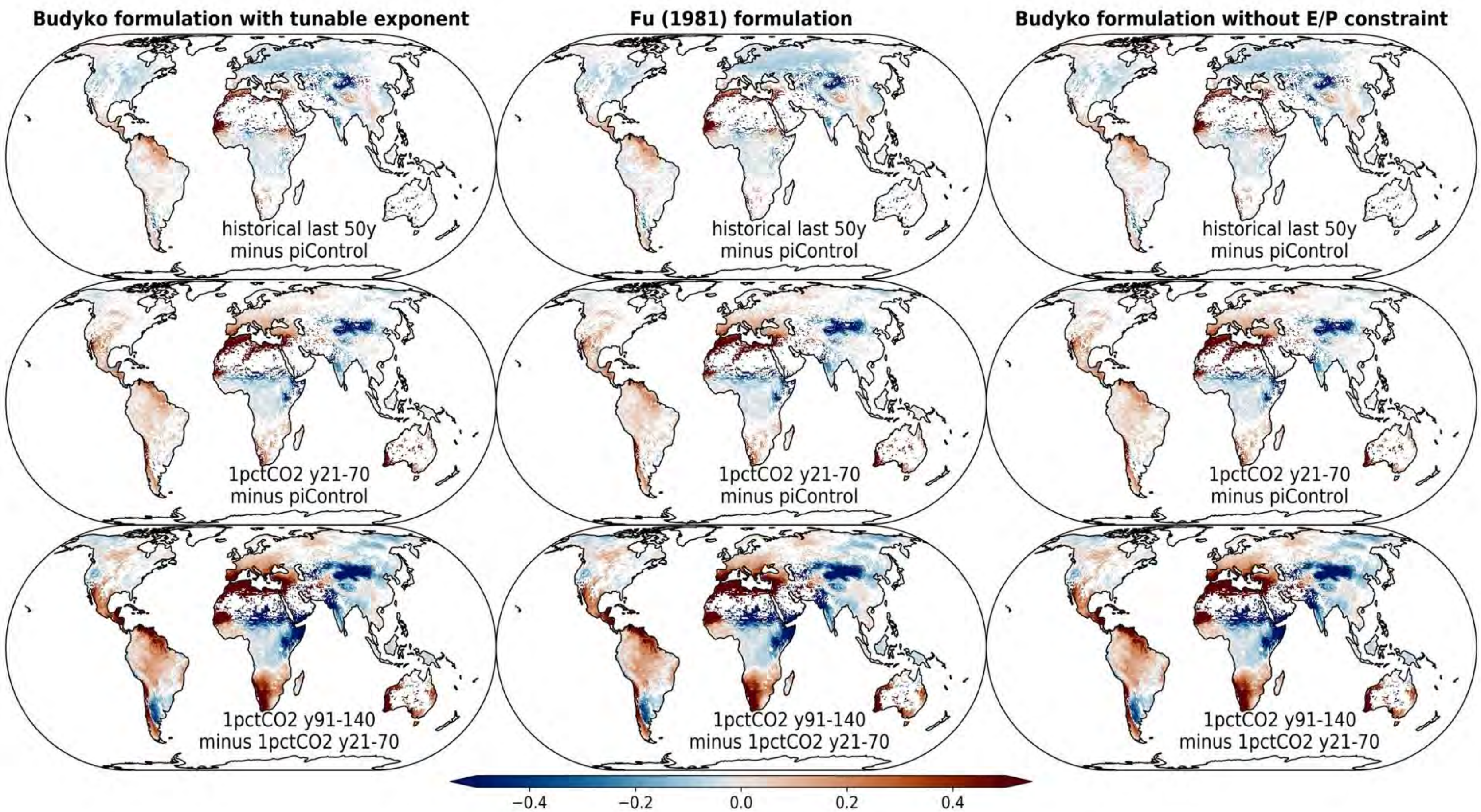

Figure S7. As in Figure S6 for the component parallel to the Budyko curve (the numerator in Figure S6).

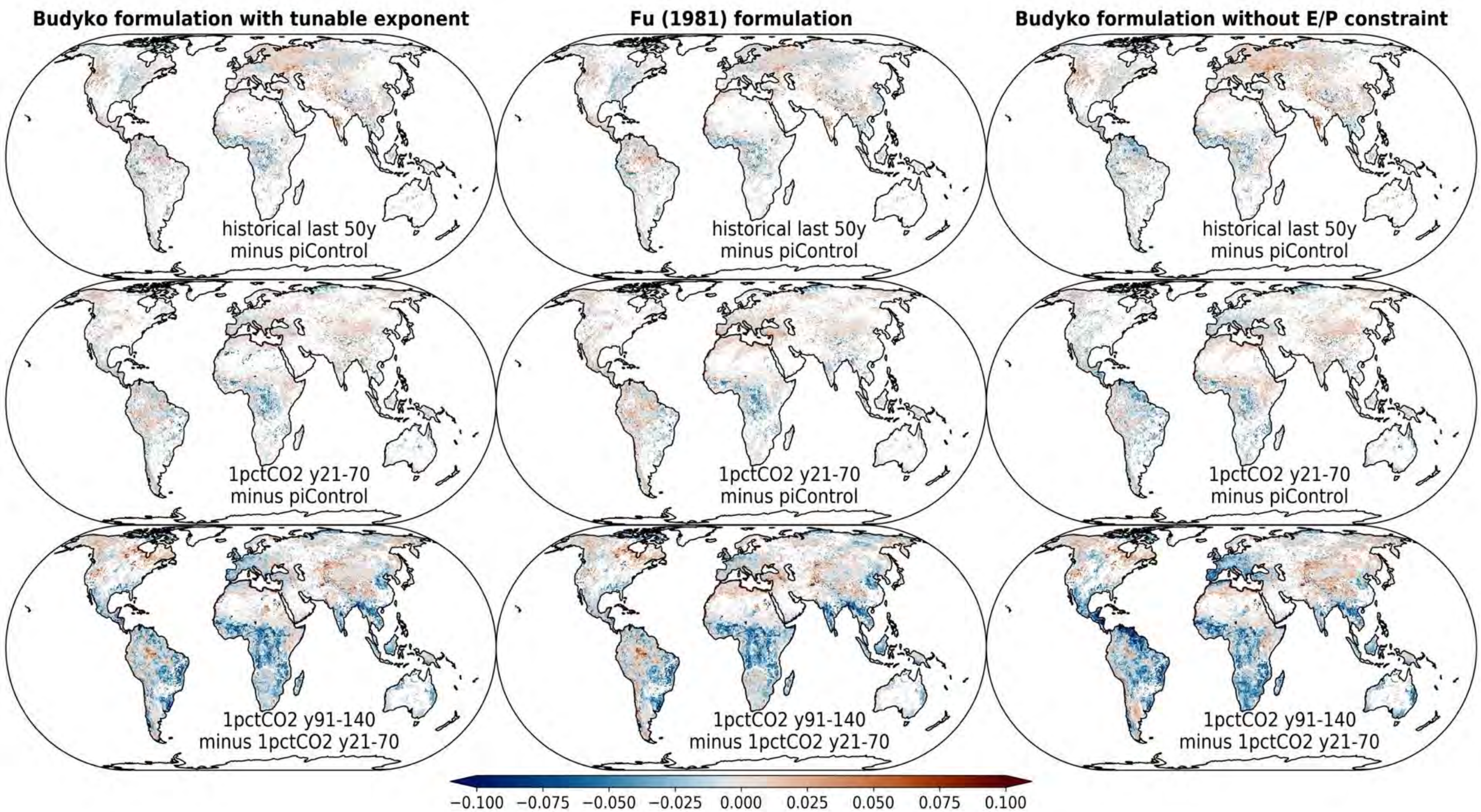

Figure S8. As in Figure S6 for the component perpendicular to the Budyko curve (the denominator in Figure S6).

Table S1: CMIP model full citations and whether the models predict vegetation phenology (Phen) or include a fully dynamic vegetation model (DVM). For some models we were unable to verify vegetation model capabilities from the literature.

CMIP Label	DVM	Phen	Full Citation
AWI-CM-1-1-MR	No	Yes	Semmler, Tido; Danilov, Sergey; Rackow, Thomas; Sidorenko, Dmitry; Barbi, Dirk; Hegewald, Jan; Sein, Dmitri; Wang, Qiang; Jung, Thomas (2018). AWI AWI-CM1.1MR model output prepared for CMIP6 CMIP. Earth System Grid Federation. doi: https://doi.org/10.22033/ESGF/CMIP6.359.
BCC-CSM2-MR	?	Yes	Xin, Xiaoge; Zhang, Jie; Zhang, Fang; Wu, Tongwen; Shi, Xueli; Li, Jianglong; Chu, Min; Liu, Qianxia; Yan, Jinghui; Ma, Qiang; Wei, Min (2018). BCC BCC-CSM2MR model output prepared for CMIP6 CMIP. Earth System Grid Federation. doi: https://doi.org/10.22033/ESGF/CMIP6.1725.
BCC-ESM1	No	Yes	Zhang, Jie; Wu, Tongwen; Shi, Xueli; Zhang, Fang; Li, Jianglong; Chu, Min; Liu, Qianxia; Yan, Jinghui; Ma, Qiang; Wei, Min (2018). BCC BCC-ESM1 model output prepared for CMIP6 CMIP. Earth System Grid Federation. doi: https://doi.org/10.22033/ESGF/CMIP6.1734.
CAMS-CSM1-0	?	?	Rong, Xinyao (2019). CAMS CAMS_CSM1.0 model output prepared for CMIP6 CMIP. Earth System Grid Federation. doi: https://doi.org/10.22033/ESGF/CMIP6.1399.
CanESM5	No	Yes	Swart, Neil Cameron; Cole, Jason N.S.; Kharin, Viatcheslav V.; Lazare, Mike; Scinocca, John F.; Gillett, Nathan P.; Anstey, James; Arora, Vivek; Christian, James R.; Jiao, Yanjun; Lee, Warren G.; Majaess, Fouad; Saenko, Oleg A.; Seiler, Christian; Seinen, Clint; Shao, Andrew; Solheim, Larry; von Salzen, Knut; Yang, Duo; Winter, Barbara; Sigmond, Michael (2019). CCCma CanESM5 model output prepared for CMIP6 CMIP. Earth System Grid Federation. doi: https://doi.org/10.22033/ESGF/CMIP6.1303.
CESM2	No	Yes	Danabasoglu, Gokhan (2019). NCAR CESM2 model output prepared for CMIP6 CMIP. Earth System Grid Federation. doi: https://doi.org/10.22033/ESGF/CMIP6.2185.
CESM2-WACCM	No	Yes	Danabasoglu, Gokhan (2019). NCAR CESM2-WACCM model output prepared for CMIP6 CMIP. Earth System Grid Federation. doi: https://doi.org/10.22033/ESGF/CMIP6.10024.
CESM2-WACCM-FV2	No	Yes	Danabasoglu, Gokhan (2019). NCAR CESM2-WACCM-FV2 model output prepared for CMIP6 CMIP. Earth System Grid Federation. doi: https://doi.org/10.22033/ESGF/CMIP6.11282.
CNRM-CM6-1	No	No	Voldoire, Aurore (2018). CNRM-CERFACS CNRM-CM6-1 model output prepared for CMIP6 CMIP. Earth System Grid Federation. doi: https://doi.org/10.22033/ESGF/CMIP6.1375.
CNRM-ESM2-1	No	?	Seferian, Roland (2018). CNRM-CERFACS CNRM-ESM2-1 model output prepared for CMIP6 CMIP. Earth System Grid Federation. doi: https://doi.org/10.22033/ESGF/CMIP6.1391.
E3SM-1-0	No	Yes	Bader, David C.; Leung, Ruby; Taylor, Mark; McCoy, Renata B. (2019). E3SM-Project E3SM1.0 model output prepared for CMIP6 CMIP. Earth System Grid Federation. doi: https://doi.org/10.22033/ESGF/CMIP6.2294.
EC-Earth3	No	?	EC-Earth Consortium (EC-Earth) (2019). EC-Earth-Consortium EC-Earth3 model output prepared for CMIP6 CMIP. Earth System Grid Federation. doi: https://doi.org/10.22033/ESGF/CMIP6.181.

CMIP Label	DVM	Phen	Full Citation
EC-Earth3-Veg	Yes	Yes	EC-Earth Consortium (EC-Earth) (2019). EC-Earth-Consortium EC-Earth3-Veg model output prepared for CMIP6 CMIP. Earth System Grid Federation. doi: https://doi.org/10.22033/ESGF/CMIP6.642.
FGOALS-g3	Yes	Yes	Li, Lijuan (2019). CAS FGOALS-g3 model output prepared for CMIP6 CMIP. Earth System Grid Federation. doi: https://doi.org/10.22033/ESGF/CMIP6.1783.
GFDL-CM4	Yes	Yes	Guo, Huan; John, Jasmin G; Blanton, Chris; McHugh, Colleen; Nikonov, Serguei; Radhakrishnan, Aparna; Rand, Kristopher; Zadeh, Niki T.; Balaji, V; Durachta, Jeff; Dupuis, Christopher; Menzel, Raymond; Robinson, Thomas; Underwood, Seth; Vahlenkamp, Hans; Bushuk, Mitchell; Dunne, Krista A.; Dussin, Raphael; Gauthier, Paul PG; Ginoux, Paul; Griffies, Stephen M.; Hallberg, Robert; Harrison, Matthew; Hurlin, William; Malyshev, Sergey; Naik, Vaishali; Paulot, Fabien; Paynter, David J; Ploshay, Jeffrey; Reichl, Brandon G; Schwarzkopf, Daniel M; Seman, Charles J; Shao, Andrew; Silvers, Levi; Wyman, Bruce; Yan, Xiaoqin; Zeng, Yujin; Adcroft, Alistair; Dunne, John P.; Held, Isaac M; Krasting, John P.; Horowitz, Larry W.; Milly, P.C.D; Shevliakova, Elena; Winton, Michael; Zhao, Ming; Zhang, Rong (2018). NOAA-GFDL GFDL-CM4 model output. Earth System Grid Federation. doi: https://doi.org/10.22033/ESGF/CMIP6.1402.
GFDL-ESM4	Yes	Yes	Krasting, John P.; John, Jasmin G; Blanton, Chris; McHugh, Colleen; Nikonov, Serguei; Radhakrishnan, Aparna; Rand, Kristopher; Zadeh, Niki T.; Balaji, V; Durachta, Jeff; Dupuis, Christopher; Menzel, Raymond; Robinson, Thomas; Underwood, Seth; Vahlenkamp, Hans; Dunne, Krista A.; Gauthier, Paul PG; Ginoux, Paul; Griffies, Stephen M.; Hallberg, Robert; Harrison, Matthew; Hurlin, William; Malyshev, Sergey; Naik, Vaishali; Paulot, Fabien; Paynter, David J; Ploshay, Jeffrey; Schwarzkopf, Daniel M; Seman, Charles J; Silvers, Levi; Wyman, Bruce; Zeng, Yujin; Adcroft, Alistair; Dunne, John P.; Dussin, Raphael; Guo, Huan; He, Jian; Held, Isaac M; Horowitz, Larry W.; Lin, Pu; Milly, P.C.D; Shevliakova, Elena; Stock, Charles; Winton, Michael; Xie, Yuanyu; Zhao, Ming (2018). NOAA-GFDL GFDL-ESM4 model output prepared for CMIP6 CMIP. Earth System Grid Federation. doi: https://doi.org/10.22033/ESGF/CMIP6.1407.
GISS-E2-1-G	No	No	NASA Goddard Institute for Space Studies (NASA/GISS) (2018). NASA-GISS GISS-E2.1G model output prepared for CMIP6 CMIP. Earth System Grid Federation. doi: https://doi.org/10.22033/ESGF/CMIP6.1400.
GISS-E2-1-H	No	No	NASA Goddard Institute for Space Studies (NASA/GISS) (2018). NASA-GISS GISS-E2.1H model output prepared for CMIP6 CMIP. Earth System Grid Federation. doi: https://doi.org/10.22033/ESGF/CMIP6.1421.
HadGEM3-GC31-LL	No	No	Ridley, Jeff; Menary, Matthew; Kuhlbrodt, Till; Andrews, Martin; Andrews, Tim (2018). MOHC HadGEM3-GC31-LL model output prepared for CMIP6 CMIP. Earth System Grid Federation. doi: https://doi.org/10.22033/ESGF/CMIP6.419.
HadGEM3-GC31-MM	No	No	Ridley, Jeff; Menary, Matthew; Kuhlbrodt, Till; Andrews, Martin; Andrews, Tim (2019). MOHC HadGEM3-GC31-MM model output prepared for CMIP6 CMIP. Earth System Grid Federation. doi: https://doi.org/10.22033/ESGF/CMIP6.420.

CMIP Label	DVM	Phen	Full Citation
INM-CM4-8	?	Yes	Volodin, Evgeny; Mortikov, Evgeny; Gritsun, Andrey; Lykossov, Vasily; Galin, Vener; Diansky, Nikolay; Gusev, Anatoly; Kostrykin, Sergey; Iakovlev, Nikolay; Shestakova, Anna; Emelina, Svetlana (2019). INM INM-CM4-8 model output prepared for CMIP6 CMIP. Earth System Grid Federation. doi: https://doi.org/10.22033/ESGF/CMIP6.1422.
INM-CM5-0	?	Yes	Volodin, Evgeny; Mortikov, Evgeny; Gritsun, Andrey; Lykossov, Vasily; Galin, Vener; Diansky, Nikolay; Gusev, Anatoly; Kostrykin, Sergey; Iakovlev, Nikolay; Shestakova, Anna; Emelina, Svetlana (2019). INM INM-CM5-0 model output prepared for CMIP6 CMIP. Earth System Grid Federation. doi: https://doi.org/10.22033/ESGF/CMIP6.1423.
IPSL-CM6A-LR	No	Yes	Boucher, Olivier; Denvil, Sébastien; Caubel, Arnaud; Foujols, Marie Alice (2020). IPSL IPSL-CM6A-LR-INCA model output prepared for CMIP6 AerChemMIP. Earth System Grid Federation. doi: https://doi.org/10.22033/ESGF/CMIP6.13581.
KACE-1-0-G	Yes	Yes	Byun, Young-Hwa; Lim, Yoon-Jin; Sung, Hyun Min; Kim, Jisun; Sun, Minah; Kim, Byeong-Hyeon (2019). NIMS-KMA KACE1.0-G model output prepared for CMIP6 CMIP. Earth System Grid Federation. doi: https://doi.org/10.22033/ESGF/CMIP6.2241.
MCM-UA-1-0	No	No	Stouffer, Ronald (2019). U of Arizona MCM-UA-1-0 model output prepared for CMIP6 CMIP. Earth System Grid Federation. doi: https://doi.org/10.22033/ESGF/CMIP6.2421
MIROC-ES2L	No	Yes	Hajima, Tomohiro; Abe, Manabu; Arakawa, Osamu; Suzuki, Tatsuo; Komuro, Yoshiki; Ogura, Tomoo; Ogochi, Koji; Watanabe, Michio; Yamamoto, Akitomo; Tatebe, Hiroaki; Noguchi, Maki A.; Ohgaito, Rumi; Ito, Akinori; Yamazaki, Dai; Ito, Akihiko; Takata, Kumiko; Watanabe, Shingo; Kawamiya, Michio; Tachiiri, Kaoru (2019). MIROC MIROC-ES2L model output prepared for CMIP6 CMIP. Earth System Grid Federation. doi: https://doi.org/10.22033/ESGF/CMIP6.902.
MIROC6	No	No	Takemura, Toshihiko (2019). MIROC MIROC6 model output prepared for CMIP6 AerChemMIP. Earth System Grid Federation. doi: https://doi.org/10.22033/ESGF/CMIP6.9121.
MPI-ESM-1-2-HAM	Yes	Yes	Neubauer, David; Ferrachat, Sylvaine; Siegenthaler-Le Drian, Colombe; Stoll, Jens; Folini, Doris Sylvia; Tegen, Ina; Wieners, Karl-Hermann; Mauritsen, Thorsten; Stemmler, Irene; Barthel, Stefan; Bey, Isabelle; Daskalakis, Nikos; Heinold, Bernd; Kokkola, Harri; Partridge, Daniel; Rast, Sebastian; Schmidt, Hauke; Schutgens, Nick; Stanelle, Tanja; Stier, Philip; Watson-Parris, Duncan; Lohmann, Ulrike (2019). HAMMOZ-Consortium MPI-ESM1.2-HAM model output prepared for CMIP6 CMIP. Earth System Grid Federation. doi: https://doi.org/10.22033/ESGF/CMIP6.1622.

CMIP Label	DVM	Phen	Full Citation
MPI-ESM1-2-HR	No	Yes	Jungclaus, Johann; Bittner, Matthias; Wieners, Karl-Hermann; Wachsmann, Fabian; Schupfner, Martin; Legutke, Stephanie; Giorgetta, Marco; Reick, Christian; Gayler, Veronika; Haak, Helmuth; de Vrese, Philipp; Raddatz, Thomas; Esch, Monika; Mauritsen, Thorsten; von Storch, Jin-Song; Behrens, Jörg; Brovkin, Victor; Claussen, Martin; Crueger, Traute; Fast, Irina; Fiedler, Stephanie; Hagemann, Stefan; Hohenegger, Cathy; Jahns, Thomas; Kloster, Silvia; Kinne, Stefan; Lasslop, Gitta; Kornblueh, Luis; Marotzke, Jochem; Matei, Daniela; Meraner, Katharina; Mikolajewicz, Uwe; Modali, Kameswarrao; Müller, Wolfgang; Nabel, Julia; Notz, Dirk; Peters, Karsten; Pincus, Robert; Pohlmann, Holger; Pongratz, Julia; Rast, Sebastian; Schmidt, Hauke; Schnur, Reiner; Schulzweida, Uwe; Six, Katharina; Stevens, Bjorn; Voigt, Aiko; Roeckner, Erich (2019). MPI-M MPIESM1.2-HR model output prepared for CMIP6 CMIP. Earth System Grid Federation. doi: https://doi.org/10.22033/ESGF/CMIP6.741.
MPI-ESM1-2-LR	Yes	Yes	Wieners, Karl-Hermann; Giorgetta, Marco; Jungclaus, Johann; Reick, Christian; Esch, Monika; Bittner, Matthias; Legutke, Stephanie; Schupfner, Martin; Wachsmann, Fabian; Gayler, Veronika; Haak, Helmuth; de Vrese, Philipp; Raddatz, Thomas; Mauritsen, Thorsten; von Storch, Jin-Song; Behrens, Jörg; Brovkin, Victor; Claussen, Martin; Crueger, Traute; Fast, Irina; Fiedler, Stephanie; Hagemann, Stefan; Hohenegger, Cathy; Jahns, Thomas; Kloster, Silvia; Kinne, Stefan; Lasslop, Gitta; Kornblueh, Luis; Marotzke, Jochem; Matei, Daniela; Meraner, Katharina; Mikolajewicz, Uwe; Modali, Kameswarrao; Müller, Wolfgang; Nabel, Julia; Notz, Dirk; Peters, Karsten; Pincus, Robert; Pohlmann, Holger; Pongratz, Julia; Rast, Sebastian; Schmidt, Hauke; Schnur, Reiner; Schulzweida, Uwe; Six, Katharina; Stevens, Bjorn; Voigt, Aiko; Roeckner, Erich (2019). MPI-M MPIESM1.2-LR model output prepared for CMIP6 CMIP. Earth System Grid Federation. doi: https://doi.org/10.22033/ESGF/CMIP6.742.
MRI-ESM2-0	No	No	Yukimoto, Seiji; Koshiro, Tsuyoshi; Kawai, Hideaki; Oshima, Naga; Yoshida, Kohei; Urakawa, Shogo; Tsujino, Hiroyuki; Deushi, Makoto; Tanaka, Taichu; Hosaka, Masahiro; Yoshimura, Hiromasa; Shindo, Eiki; Mizuta, Ryo; Ishii, Masayoshi; Obata, Atsushi; Adachi, Yukimasa (2019). MRI MRI-ESM2.0 model output prepared for CMIP6 CMIP. Earth System Grid Federation. doi: https://doi.org/10.22033/ESGF/CMIP6.621.
NESM3	Yes	Yes	Cao, Jian; Wang, Bin (2019). NUIST NESMv3 model output prepared for CMIP6 CMIP. Earth System Grid Federation. doi: https://doi.org/10.22033/ESGF/CMIP6.2021.
NorCPM1	?	?	Bethke, Ingo; Wang, Yiguo; Counillon, François; Kimmritz, Madlen; Fransner, Filippa; Samuelsen, Annette; Langehaug, Helene Reinertsen; Chiu, Ping-Gin; Bentsen, Mats; Guo, Chuncheng; Tjiputra, Jerry; Kirkevåg, Alf; Olivià, Dirk Jan Leo; Seland, Øyvind; Fan, Yuanchao; Lawrence, Peter; Eldevik, Tor; Keenlyside, Noel (2019). NCC NorCPM1 model output prepared for CMIP6 CMIP. Earth System Grid Federation. doi: https://doi.org/10.22033/ESGF/CMIP6.10843.

CMIP Label	DVM	Phen	Full Citation
NorESM2-LM	No	Yes	Seland, Øyvind; Bentsen, Mats; Oliviè, Dirk Jan Leo; Toniazzo, Thomas; Gjermundsen, Ada; Graff, Lise Seland; Debernard, Jens Boldingh; Gupta, Alok Kumar; He, Yanchun; Kirkevåg, Alf; Schwinger, Jörg; Tjiputra, Jerry; Aas, Kjetil Schanke; Bethke, Ingo; Fan, Yuanchao; Griesfeller, Jan; Grini, Alf; Guo, Chuncheng; Ilicak, Mehmet; Karset, Inger Helene Hafsahl; Landgren, Oskar Andreas; Liakka, Johan; Moseid, Kine Onsum; Nummelin, Aleksi; Spensberger, Clemens; Tang, Hui; Zhang, Zhongshi; Heinze, Christoph; Iversen, Trond; Schulz, Michael (2019). NCC NorESM2-LM model output prepared for CMIP6 CMIP. Earth System Grid Federation. doi: https://doi.org/10.22033/ESGF/CMIP6.502.
SAM0-UNICON	No	Yes	Park, Sungsu; Shin, Jihoon (2019). SNU SAM0-UNICON model output prepared for CMIP6 CMIP. Earth System Grid Federation. doi: https://doi.org/10.22033/ESGF/CMIP6.1489.
TaiESM1	No	Yes	Lee, Wei-Liang; Liang, Hsin-Chien (2019). AS-RCEC TaiESM1.0 model output prepared for CMIP6 CMIP. Earth System Grid Federation. doi: https://doi.org/10.22033/ESGF/CMIP6.9684.
UKESM1-0-LL	Yes	Yes	Tang, Yongming; Rumbold, Steve; Ellis, Rich; Kelley, Douglas; Mulcahy, Jane; Sellar, Alistair; Walton, Jeremy; Jones, Colin (2019). MOHC UKESM1.0-LL model output prepared for CMIP6 CMIP. Earth System Grid Federation. doi: https://doi.org/10.22033/ESGF/CMIP6.1569.